Stable, static Curvature-cosmology

David F. Crawford[1]

[1]*School of Physics (Retired), University of Sydney, NSW, 2006, Australia*

(Dated: August 6, 2022)

ABSTRACT

This paper describes Curvature-cosmology that is a tired-light cosmology that predicts a well-defined static and stable universe. It provides a new simpler raw data analysis for Type Ia supernova. Since it is a complete challenge to the big bang paradigm, Curvature-cosmology can only be judged by its agreement with direct cosmological observations. Curvature-cosmology predicts a universe of a hydrogen plasma with a temperature of 2.456×10^9 K [observed: 2.62×10^9K] and a cosmic background radiation temperature of 2.736 K [observed: 2.725K]. It has only one parameter which is the density of the cosmic plasma. The major observations that are shown to consistent with it are: Type 1a supernova, Tolman surface density, brightness, angular size, galaxy distributions, X-ray background radiation, and quasar variability. It does not need inflation, dark matter or dark energy.

Keywords: cosmology, supernova

Contents

email: davdcraw@gmail.com

1. INTRODUCTION

This paper describes the Curvature-cosmology paradigm that challenges the big bang paradigm to see which provides the best agreement with cosmological observations. Following the precepts of Thomas S. Kuhn (Kuhn 1970) it is essential that each paradigm must be judged using its own analysis. That is observations of non-static behavior observed within the old paradigm cannot be used to invalidate the new paradigm. They must be evaluated within the new paradigm to have any validity.

Curvature-cosmology has excellent agreement with all the major cosmological observations and a brief summary is provided in Table 1.

Nearby Type Ia supernova are well known to have essentially identical light curves that make excellent cosmological probes. The observational evidence for their time dilation has a long history with notable papers being by Goldhaber et al. (2001, 1996); Blondin et al. (2008). More recent contributions are by Kowalski et al. (2008); Wood-Vasey et al. (2008); Kessler et al. (2009a); Amanullah et al. (2010); Conley et al. (2011); Betoule et al. (2014); Scolnic et al. (2018). All of these recent papers use the SALT2 Guy et al. (2010, 2007) method to determine the widths and peak flux densities of the supernova and they have used the ΛCDM expansion cosmology to determine absolute magnitudes. These papers show that type Ia supernova observations provide the major contribution to cosmological models.

The common attribute of all ΛCDM , cosmologies is that they are based on the assumption that the universe is expanding (Peebles 1993). An early alternative was the steady-state theory of Hoyle, Bondi and Gold Hoyle (1962) (described with later extensions by Hoyle et al. (2000)) that required continuous creation of matter. However steady-state theories have serious difficulties in explaining the cosmic microwave background radiation. This left ΛCDM as the dominant cosmology but still subject to criticism.

Lal (2010) and Joseph (2010) have continued major earlier criticisms of ΛCDM cosmologies (Ellis 1984; Lerner 1991; Disney 2000; van Flandern 1991). Whereas most of these criticisms have been of a theoretical nature, this paper concentrates on whether observational data supports a static cosmological model, Curvature-cosmology.

A crucial property of Curvature-cosmology is that the observed magnitude is the sum of an intrinsic magnitude, which is what would be observed by a nearby observer and a cosmological magnitude. The cosmological magnitude is a comes from the change in the average energy of the photons due to their trajectory through the universe. Whereas the intrinsic magnitude is only a property of the observed object and is completely independent of the cosmology.

This paper has three major parts where the first part presents a new much simpler method that analyzes raw Type Ia supernova data in order to measure their light curve widths and their peak flux densities. These results are compared with the standard SALT2 method and it showed that the SALT2 method (summarized in the appendix) has a flaw in its flux density results.

The second part presents a new static cosmology, Curvature-cosmology, that has excellent agreement with observations.

The third part provides the observation data for many cosmological observations and discuses their results in the context of Curvature-cosmology.

This paper is the culmination of many years of work and is a complete re-synthesis of many approaches that I have already published (Crawford 1987a,b, 1991, 1993, 1995a,b, 1998, 1999a,b, 2006, 2009a,b). These papers are cited to show the convoluted and historical path of Curvature-cosmology. Because hypotheses and notations have changed and evolved, direct references to these earlier versions of the theory would be misleading and all relevant results are published in this paper.

For convenience it is assumed that the wavelength dependence of a band can be replaced by a single value, λ, which is the mean wavelength for that band.

2. CONCLUSIONS

The major tests for Curvature-cosmology is shown in Table 1.

The major support for the λCDM model is that it describes the general relativity model of an unstable expanding universe. This is similar to assuming that a falling feather should have the same acceleration as a falling stone, whereas we know that the difference is due to air resistance. Maybe cosmology needs something like air resistance such as Curvature-cosmology,

Crucially the standard procedure is to use λCDM or one of its variants to determine the dimensionless density parameters, which depend on assumptions of inflation, dark matter and dark energy. Since none of these properties are substantiated by other independent observations, they do not provide any support for this cosmology. Moreover they are ad hoc models largely determined by supernova observations. In other words, there are no observations other than those for supernova that show strong confirmation of the SALT2 analysis and the λCDM model.

Curvature-cosmology is a static tired-light cosmology which is a static solution to the equation of general rel-

Table 1. Predicted and observed results for Curvature-cosmology.

Cosmological measurement	Ref.	Predicted	Observed
Quasar energy loss rate	3.6	1+z	$(1.0073 \pm 0.0046)(1+z)$
Cosmic temperature	4.7	2.456×10^9 K	$(2.62 \pm 0.13) \times 10^9$ K
Supernova light curve width	3.4	1+z	$(1.060 \pm 0.009) + (1.080 \pm 0.042)\,z$
Supernova absolute magnitude M(z)	5.1	$M_0 + 0z$	$(-18.6562 \pm 0.009) + (0.081 \pm 0.057)z$
CMBR temperature	5.3	(2.736 ± 0.092) K	(2.72548 ± 0.00057) K
Tolman surface density exponent	5.4	1	(1.38 ± 0.13)

ativity that is described by the Friedmann equations with an additional term that stabilizes the solution. This term called Curvature-pressure is a reaction of high-speed particles back on the material producing the curved space-time. This sense of this reaction is to try and reduce the curvature.

The basic cosmological model is one in which the cosmic plasma dominates the mass distribution and hence the curvature of space-time. In this first-order model, the gravitational effects of stars and galaxies are neglected. The geometry is that of a three-dimensional "surface" of a four-dimensional hyper-sphere, which is common to most cosmologies. Its main strengths are that it does not have ad hoc additions to the model and it has exceptionally good agreement with cosmological observations.

This is a brief summary of the quantitative observations that are relevant to the Curvature-cosmology model. The predicted Hubble's constant is $H_0 = 41.30 \ \mathrm{kms}^{-1}\mathrm{Mpc}^{-1}$ where the density has used $N_H = 1.93$ from section 5.2. This value is significantly less than the current value of $h \approx 70$. However these measurements were based the standard model. A valid test would be re-evaluate the observations using Curvature-cosmology.

Curvature-cosmology does not need dark matter to explain the velocity dispersion in clusters of galaxies or the shape of galactic rotation curves. Furthermore it is shown in section 3.7 that dark energy could be due to fault in the SALT2 analysis.

For angular size the conclusion is in favor of Curvature-cosmology.

An analysis of many galaxies that have multiple observed bands show no evidence of evolution.

Curvature-cosmology predicts the observed quasar epoch variability of zero.

The Butcher-Oemler effect remains uncertain, and therefore does not provide evidence to refute a static cosmology.

Not only can Curvature-cosmology explain the anomalous Pioneer 10 acceleration, it has a feasible prediction of its value.

Fluctuations in the CMBR can be explained a density fluctuations in the cosmic plasma.

Overall for Curvature-cosmology there is remarkable agrement between its predictions and observations, without any serious problems.

3. PART A: ANALYSIS OF TYPE IA SUPERNOVA

3.1. *Introduction*

This part describes a new analysis method (intrinsic analysis) for Type Ia supernova that is simple and can replace the standard SALT2 method. A major difference from SALT2 is that it explicitly estimates and uses intrinsic flux densities.

It is shown that absolute magnitudes of Type Ia supernova analyzed with the SALT2 method and using the λCDM distance modulus are independent of redshift. However supernova analyzed with the intrinsic analysis and using the λCDM distance modulus have a significant dependence on redshift which implies a fault in the SALT2 analysis .

Although the intrinsic magnitude is the same as the absolute magnitude, the different name is used because the measurement method is different. The intrinsic magnitude can only be used when there are many bands and relies on the fact that each **band** must have the same cosmological magnitude. Whereas using a distance modulus, the absolute magnitude can be applied to a single observation.

The next section covers the results for intrinsic magnitudes for both Type Ia supernova and quasars. An important product is plots of intrinsic magnitudes verses intrinsic wavelengths, both of which appear to be dominated by atomic hydrogen absorption.

Although the absolute magnitudes for supernova analyzed with the SALT2 method and the λCDM model show no dependence with redshift. The absolute magnitudes for intrinsic analysis and the λCDM model are

4

significantly different from zero. Section 3.7 provides a discussion of why the λCDM model may be flawed.

3.2. Type Ia supernova

From WikipediA: "Type Ia Supernova is believed to result from mass accretion to a carbon-oxygen white dwarf in a close binary system. When the white dwarf mass exceeds the Chandrasekhar limit, the degenerate electron pressure can no longer support the accumulated mass and the star collapses in a thermonuclear explosion producing a supernova. The peak luminosity of supernova Ia is set by the radioactive decay chain, and the observed photometric correlation between the peak luminosity and the time-scale over which the light curve decays from its maximum is understood physically as having both the luminosity and opacity being set by the mass of Nickel-56 synthesized in the explosion.

The major observational evidence for Type Ia supernova is a lack of hydrogen lines and a singly ionized silicon (Si II) absorption feature at 0.615μ m near peak brightness."

The observation of a distant supernova requires the emission of a photon from an intrinsic source and then it follows a trajectory that is determined by the geometry of the universe. If the universe is expanding then their average energy is determined by velocity of the telescope relative to the source. If the universe is static, this energy loss could be the result of photons being scattered outside the beam.

A critical part in measuring the light curve width of Type Ia supernova light curves is to have a reference light curve. The observed light curve must have the same shape independent of redshift. Only its width and height will vary with redshift. Consequently this property is assumed in intrinsic analysis.

In order to remove any possible bias, a standard independent template, the B band Parab-18 from Table 2 from Goldhaber et al. (2001) which has the first half-peak width at -10.1 days and the second half-peak width at 22.3 days is used. Consequently all widths are relative to this light curve.

The purpose of the light-curve analysis is to obtain estimates of the peak flux density for each band, the width (common to all bands) of the light-curve relative to the template and the epoch offset of the light curve. This offset is a nuisance parameter that allows for the unknown epoch of the peak flux density and is defined to be the epoch difference between the fitted light curve relative to the observed epochs.

An initial problem is to determine the initial epoch offset q. The solution used was to estimate the average flux density for every epoch in the observed range.

This averaging used a Gaussian weight factor with the $weight = \exp(-0.5(p_i - q)^2)$ where p_i is the epoch of an observation and q is the reference epoch. The day with the largest average flux density defined the initial epoch offset.

The intrinsic analysis method starts with the observed flux density, f_i for the index i, and its uncertainty σ_i. Then for each supernova and each band the maximum likelihood method is used to determine the fitted maximum flux density, F and its epoch.

Let the reference supernova light curve be referenced by $C((p_i - q)/w)$ where p_i is the epoch, w is the computed width, and q is the epoch offset of the maximum of the fitted light curve. Then, assuming a Gaussian flux density noise distribution, the log-likelihood function for a single band, with n observations, of a supernova is

$$\mathcal{L} = \sum_{i=1}^{n}\left[\left(\frac{f_i - b - F \times C((p_i - q)/w)}{\sigma_i}\right)^2\right], \quad (1)$$

where i is the observation index, the epoch is p_i and b is the base flux density level for the current band. A constant term that depends only on the measurement uncertainties is omitted. Additionally the omission of the factor $-1/2$ means that $\mathcal{L}$ is a ψ^2 variate with n degrees of freedom. Thus the maximization of the likelihood is identical to the minimization of $\mathcal{L}$.

Although the peak flux density and base level are determined by an analytic fit, the values for the epoch offset and width are easily found by numerical minimization. Fortunately, the flux density and width are almost orthogonal so that a sequence of alternate fits rapidly converges.

Note that in Eq 1 each flux density and each peak flux density is divided by its uncertainty which means that the fitted width is independent of individual band calibrations and all bands can be included in the same expression.

All the information about the width distribution is contained in $\mathcal{L}$. The uncertainty in the width was determined from the proposition that the likelihood function, $\mathcal{L}$ as a function of width is equal to the likelihood of a Gaussian function of width with a standard deviation equal to the width uncertainty. That is

$$\mathcal{L} = (\frac{w}{\sigma_w})^2, \quad (2)$$

where w is the width and σ_w is the estimated uncertainty in the width and it is estimated using Eq. 1.

It must be noted that the fitting procedure is completely independent of the redshift and is also independent of the band type. Although each band had its own estimate of its peak flux density, the width is the result

of a common fit to all observations for each supernova. Thus the computed parameters for each supernova are its light curve width, and the peak flux density for each band which is the flux density for that band at the maximum epoch of the common fitted light curve.

3.3. *The observations.*

The Type Ia supernova data used here comes from the Supernova Legacy survey (SNSL), the Sloan Digital Survey (SDSS) (both sourced from the SNANA website Kessler et al. (2009b)), and the Panoramic Survey Telescope and Rapid Response System, (Pan-STARRS), supernova survey Kaiser et al. (2010); Jones et al. (2018); Scolnic et al. (2018) and those observed by the Hubble Space Telescope (HST) Riess et al. (2007); Jones et al. (2013).

The observations of Type Ia supernova from Pan-STARRS, (PS1), were accessed from the site https://archive.stsci.edu/prepds/ps1cosmo/jones and the file datatable.html. In 2018 Pan-STARRS consisted of two 1.8-m Ritchey-Chrétien telescopes located at Haleakala in Hawaii and could record almost 1.4 billion pixels per image. It is designed to detect moving or variable objects on a continual basis. An image with a 30 to 60 second duration can record down to an apparent magnitude of 22 mag. The whole visible sky will be surveyed four times a month.

Although theoretically, the Type Ia supernova model has a fixed absolute magnitude, its measurement is subject to the usual uncertainties. This is why they can be observed at redshifts beyond the nominal limit of the telescope and are subject to Malmquist bias.

However many of the observations come from the PS1 survey which is essentially providing a continuous record of the sky so that the simple Malmquist bias is not applicable. However for all the other supernova a Malmquist bias is $-1.382\sigma_i^2$ mag, where σ_i is the observed flux density uncertainty. But since application of Malmquist bias corrections made negligible difference to the results it has not been applied.

Table 2 shows the statistics for the selected supernova. The selection criteria was that there was a good fit and the width was between 0.3 and 5.0 and the width uncertainly was less than 0.3. In addition the value of $\mathcal{L}$ had to be less than $20/n$.

3.4. *Results for the light curve width*

from $1,745$ initial candidates there were $1,707$ that satisfied the selection criteria. Most of the rejections were because there were insufficient observations prior to the peak epoch.

The important result of this width analysis is a regression of $w_{obs}(z)$ as a function of z for all the $1,707$

Table 2. Light-curve numbers for each band

Band	$\lambda/\mu\,\mathrm{m}$	N[a]	N[b]
U	0.365	77	0
B	0.445	121	0
V	0.551	121	0
R	0.658	72	0
I	0.809	74	0
u	0.354	141	0
g	0.475	421	1141
r	0.622	468	1132
i	0.763	468	1142
z	0.905	412	1146
F775W	0.771	7	0
F850LP	0.907	17	0

[a] Number of supernova from other catalogues.
[b] Number of supernova for the PS1 catalogue.

accepted observations which is

$$w_{obs}(z) = (1.060 \pm 0.009 + (1.080 \pm 0.042))\,z. \quad (3)$$

Although the ordinate is statistically different from one, it is this ordinate that is most sensitive to calibration and systematic errors such as having minor errors in the reference light curve. Here this difference is not important. However the coordinate shows an excellent agreement with one. Note that this width measurement is independent any cosmological model.
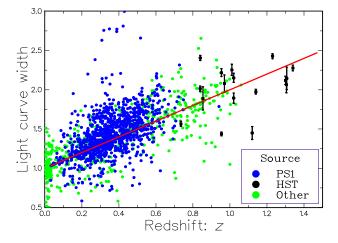
The widths for all the supernova are shown in Figure 1. It is clear that the slope is consistent with the expected dependence of $w(z) = 1+z$. Some of the supernova show either discrepant widths or discrepant uncertainties and to avoid any bias, no rejections have been made to the original data.

For convenience it helps to convert all the flux densities into magnitudes. All computed apparent magnitudes except the those in the SDSS catalogue were calculated by $m_k = 27.5 - 2.5\log_{10}(F_k)$ where F_k is the peak flux density and k is the band. Those in the SDSS catalogue had $m_k = 24.5 - 2.5\log_{10}(F_k)$.

Since each supernova has a peak flux density for each observed band, they can be combined to provide a peak intrinsic flux density for each band and a cosmological flux density for the supernova. Thus there is a clear separation between the intrinsic flux density which is independent of the redshift and the cosmological redshift that is only a function of redshift.

3.5. *Intrinsic supernova magnitudes*

Then for each supernova and band the fitted apparent magnitude is the sum of an intrinsic magnitude and a

Figure 1. A plot of the Type Ia supernova light curve observed widths. The blue dots are for the PS1 and the black dots with error bars show the HST (Hubble Space Telescope) observations. All other observations are shown by the green dots. The red line shows a $(1+z)$ dependence

common cosmological magnitude. Starting with a constant intrinsic flux density, the average magnitude was determined by fitting a regression equation to the observed peak magnitudes minus the current intrinsic magnitude which is common to all the supernova and is a function of the intrinsic wavelength.

The first step is to estimate an initial cosmological flux density as the mean of the observed peak flux densities for each band. The next step is to determine an estimate of the intrinsic flux density as a function of the intrinsic wavelength, ψ which by definition is

$$\psi = \lambda/(1+z). \qquad (4)$$

Initially there 30 boxes that cover the ψ range are set to zero, then the difference between each observed flux density and the current estimate of the cosmological magnitude is added to the appropriate box. After all the observations are processed, the procedure is repeated with each peak flux density being corrected for the average flux density defined by the mean of its box. Then a new set of cosmological magnitudes are produced. This process is repeated until there are no significant changes in the values.

Thus each supernova, the observed peak band magnitudes are reduced to a peak cosmological magnitude and a common intrinsic magnitude distribution. The individual intrinsic peak magnitude data points for the supernova are shown in Figure 2 and tabulated in Table 3. There is a very rapid decrease in the intrinsic luminosity as the intrinsic wavelength approaches the Lyman$_\alpha$ line which suggests scattering in a local hydrogen cloud. This could also explain the lack of hydrogen

Table 3. Intrinsic magnitude of Type Ia supernova

box	number	ψ/μm	magnitude
8	26	0.243	3.876$\pm$ 0.247
9	132	0.269	2.021$\pm$ 0.077
10	256	0.304	1.113$\pm$ 0.051
11	471	0.334	0.613$\pm$ 0.032
12	608	0.364	0.080$\pm$ 0.027
13	470	0.400	-0.181$\pm$ 0.022
14	521	0.434	-0.227$\pm$ 0.021
15	537	0.467	-0.197$\pm$ 0.021
16	493	0.500	-0.182$\pm$ 0.023
17	499	0.534	-0.067$\pm$ 0.030
18	498	0.567	-0.126$\pm$ 0.033
19	453	0.600	-0.114$\pm$ 0.029
20	383	0.634	0.027$\pm$ 0.039
21	368	0.667	0.086$\pm$ 0.038
22	265	0.699	0.126$\pm$ 0.042
23	190	0.733	0.443$\pm$ 0.059
24	106	0.765	0.366$\pm$ 0.084
25	100	0.798	0.520$\pm$ 0.093

lines in the spectra. Note that the size of this cloud would be very small and would not be easily detected.

Figure 2. The intrinsic peak magnitude of Type Ia supernova as a function of intrinsic wavelength, ψ. The black points and curve show the average intrinsic peak magnitude as a function of intrinsic wavelength. The bands $UBVRI$ have the same sequential colors as the bands $ugriz$. The position of the Lyman$_\alpha$ line is shown in blue.

3.6. *Intrinsic quasar magnitudes*

The purpose of this section is to show that an analysis of the observed magnitudes for many quasars is to show that they all have a relative energy loss proportional to $(1+z)$.

From WikipediA: "A quasar also known as a quasi-stellar object is an extremely luminous active galactic nucleus (AGN), powered by a supermassive black hole, with mass ranging from millions to tens of billions times the mass of the Sun, surrounded by a gaseous accretion disc. Gas in the disc falling towards the black hole heats up because of friction and releases energy in the form of electromagnetic radiation. The radiant energy of quasars is enormous; the most powerful quasars have luminosities thousands of times greater than a galaxy such as the Milky Way. Usually, quasars are categorized as a subclass of the more general category of AGN. The redshifts of quasars are of cosmological origin."

All quasar data used here is taken from the Sloan Digital Sky Survey Quasar Catalog: Sixteenth Data Release (DR16Q) Lyke et al. (2020).

The majority of these quasars gave been discovered by a flux density limited survey without knowledge of the redshift and it is clear that the observed magnitudes have a very limited dependence on their observed redshift. Thus the observation model is that the selection of each quasar is determined by the cut-off flux density and the overall telescope noise and it is assumed that these values are the same for all the quasars.

Thus for each quasar discovered its apparent magnitude must lie in the range of magnitudes that are accepted by the telescope and it is completely independent of the intrinsic magnitude of the quasar. The observed flux density depends on the probability of seeing the quasar and its distance. Since the observed distance is rapidly increasing with redshift, it is proportional to the maximum area. For this distance the observed flux density is inversely proportional to the same area. Since these two areas cancel each other, the expected flux density is the cut-off flux density plus, if any, common cosmological flux density.

The data for each quasar is its redshift and the observed magnitudes for the 5 bands, $UBVRI$. The intrinsic magnitude for each band is determined by the procedure described in section 3.3 for the supernova, except there were 1000 boxes.

The quasar intrinsic magnitude is shown in Figure 3. The rapid decrease in luminosity at short wavelengths is probably due to a local hydrogen cloud. Note that if quasars are like black holes then the size of this cloud could be very small and it would not easily be detected against the luminosity of the accretion disk.

If the universe is expanding then this energy loss factor is proportional to $(1+z)^{-1}$. A simple method to measure this average energy loss is to assume that the expected magnitude is

$$m = a + b \times 2.5 log_{10}(1+z). \qquad (5)$$

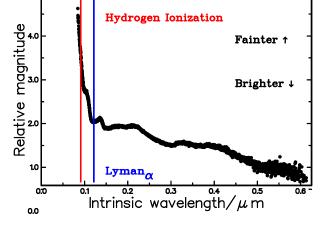**Figure 3.** The black plot shows the average intrinsic magnitude of SDSS quasars as a function of intrinsic wavelength, ψ. The position of the wavelength for the Lyman$_\alpha$ line is shown in blue and that for the hydrogen ionization is shown in red.

Then the expected values are $a = -1$ and $b = -1$. The weighted regression equation for 635,218 quasars produced the results $a = -0.9109 \pm 0.001$ and

$$b = -(1.0073 \pm 0.0046). \qquad (6)$$

The difference of the parameter a from -1 is unknown but fortunately it is not important here. However the agreement of parameter b with -1 is very clear and shows very strong support for an energy loss rate of $(1 + z)$.

The absolute magnitude of Type Ia supernova is the sum of the apparent magnitude and a distance modulus. Scolnic et al. (2017) suggests several distance moduli that have a good fit to the PS1 Medium Deep Survey that were analyzed with the SALT2 method. The simplest is the oCDM model. There are two sets of data, the 1117 PS1 set and the combined 1652 described above that can be used to test the absolute magnitude dependence on redshift. The PS1 set (JonesJones et al. (2018) table (3)) is a list of results from the Pan-STARRS supernova survey and their apparent magnitudes have been corrected using Scolnic et al. (2017) Eq.(3) and using the oCDM model, the regression of the absolute magnitude verse redshift for the 1117 PS1 Type Ia supernova that used the SALT2 model

$$M(z) = -19.205 \pm 0.009 + (0.052 \pm 0.067)z, \qquad (7)$$

where the last term is statistically equal to zero. This shows that the SALT2 method is consistent with the oCDM model.

However the regression for the 1652 PS1 Type Ia supernova, using the intrinsic analysis and the oCDM

model, is

$$M(z) = -18.562 \pm 0.009 + (0.669 \pm 0.059)z, \qquad (8)$$

where the last term is not equal to zero.

3.7. *Discussion of SALT2 magnitudes.*

The absolute magnitudes of PS1 supernova that are analyzed by the SALT2 method and using the oCDM model show negligible dependence on redshift. However the absolute magnitudes that are obtained from intrinsic analysis and using the oCDM model shows a statistically valid dependence on redshift, $\Delta M = (0.833 \pm 0.072)z$ that is inconsistent with the expected value of zero,

Could this be due to a fault in the intrinsic analysis? Because the intrinsic analysis is completely independent of the observed redshift the anomaly must be present in the observed data and cannot come from the analysis. Although it is not an independent result, section 5.21 shows that there is no Phillip's relation. The conclusion is that it must be in SALT2 and that the λCDM procedure of determining the dimensionless density parameters counteracts the fault.. As shown in the appendix the SALT2 method calibrates a new Type Ia supernova by comparing its observations against the results for previous supernova measurements, these results only show self-consistency and do not provide validation of the flux densities. However if there is a systematic error in the previous supernova measurements, it will be transmitted to new observations. Furthermore it explicitly includes the nuisance parameter α that is a measure of the Phillip's relation between magnitude and redshift.

The major support for the λCDM model is that it describes the general relativity model of an unstable expanding universe. This is similar to assuming that a falling feather should have the same acceleration as a falling stone, whereas we know that the difference is due to air resistance and is not due to a deficiency in the gravitational model. Maybe cosmology needs something like air resistance such as Curvature-cosmology,

Crucially the standard procedure is to use oCDM or one of its variants to determine the dimensionless density parameters, which depend on assumptions of inflation, dark matter and dark energy. Since none of these properties are substantiated by other independent observations, they do not provide any support for this cosmology. Moreover they are ad hoc models largely determined by supernova observations. In other words, there are no observations other than those for Type IA supernova that show strong confirmation of the SALT2 analysis and the λCDM model.

4. PART B: CURVATURE-COSMOLOGY THEORY.

4.1. *Introduction*

Curvature-cosmology is a static tired-light cosmology which is based on the two hypothesizes of Curvature-redshift which is based on the propagation of a wave in of curved space-time and Curvature-pressure which opposes the mutual gravitational attraction of hot gases.

It is a static solution to the equation of general relativity that is described by the Friedmann equations with an additional term that stabilizes the solution. This term called Curvature-pressure is a reaction of high-speed particles back on the material producing the curved space-time. This sense of this reaction is to try and reduce the curvature.

The basic cosmological model is one in which the cosmic plasma dominates the mass distribution and hence the curvature of space-time. In this first-order model, the gravitational effects of stars and galaxies are neglected. The geometry is that of a three-dimensional "surface" of a four-dimensional hyper-sphere, which is common to most cosmologies.

For a static universe, there is no ambiguity in the definition of distances and times. One can use a universal cosmic time and define distances in light travel times or any other convenient measure. In a statistical sense Curvature-cosmology obeys the perfect cosmological principle of being the same at all places and at all times.

Curvature-cosmology makes quite specific predictions that can be refuted. Thus, any observations that unambiguously show changes in the universe with a redshift would invalidate it. In Curvature-cosmology, there is a continuous process in which some of the cosmic gas will aggregate to form galaxies and then stars. The galaxies and stars will evolve and eventually all their material will be returned to the cosmic plasma. Thus, a characteristic of Curvature-cosmology is that although individual galaxies will be born, live and die, the overall population will be statistically the same for any observable characteristic.

4.2. *Derivation of Curvature-redshift*

The derivation of Curvature-redshift is based on the fundamental hypothesis of Einstein's general theory of relativity that space is curved. As a consequence, the trajectories of initially parallel point particles, geodesics, will move closer to each other, or further apart as time increases. Consequently in space with a positive curvature, the cross-sectional area of a bundle of geodesics will slowly decrease.

In applying this idea to photons, we assume that a photon is described in quantum mechanics as a localized wave where the geodesics correspond to the rays of

the wave. Note that this wave is quite separate from an electromagnetic wave that corresponds to the effects of many photons. It is fundamental to the hypothesis that we can consider the motion in space of individual photons.

Because the curvature of space causes the focusing of a bundle of geodesics, this focusing also applies to a wave. As the photon progresses, the cross-sectional area of the wave associated with it will decrease. However, in quantum mechanics properties such as angular momentum are computed by an integration of a radial coordinate over the volume of the wave and will be affected by the focusing.

If the cross-sectional area of the wave decreases, then the angular momentum will also decrease. However, angular momentum is a quantized parameter that for photons has a fixed value. The solution to this dilemma is that, from symmetry, the photon splits into two very low-energy photons and a third that has the same direction as the original photon and nearly all the energy.

Since in quantum mechanics protons and other particles are considered as waves, a similar process will also apply. It is argued that protons and other particles will interact with curved space to lose energy by the emission of very low-energy photons.

Einstein's general theory of relativity requires that the metric of space-time be determined by the distribution of mass (and energy). In general this space-time will be curved such that in a space of positive curvature, nearby geodesics that are initially parallel will come closer together as the reference position moves along them. This is directly analogous to the fact that on the earth lines of longitude come closer together as they go from the equator to either pole. In flat space-time, the separation remains constant.

The *equation for geodesic deviation* can be written Misner, Thorne, & Wheeler (1973) as

$$\frac{d^2\xi}{dr^2} = -\frac{\xi}{R^2},$$

where ξ is a distance normal to the trajectory and r is measured along the trajectory. The quantity $1/R^2$ is the Gaussian curvature at the point of consideration.

Assume that a photon can be described by a localized wave packet that has finite extent both along and normal to its trajectory. This economic description is sufficient for the following derivation. From de Broglie's equation the frequency of a photon with energy E is $\nu = E/h$ and its wavelength as $\lambda = hc/E$ where E is its energy. These definitions do not imply that we can ascribe a frequency or a wavelength to an individual photon; they are properties of groups of photons. The derivation requires that the wavelength is short compared to the size of the wave

packet and that this is short compared to variations in the curvature of space-time.

Furthermore, we assume that the rays follow null geodesics and therefore any deviations from flat space-time produce change in shape of the wave packet. In other words, since the scale length of deviations from flat space are large compared to the size of the wave packet they act as a very small perturbation to the propagation of the wave packet.

Consider a wave packet moving through a space-time of constant positive curvature. Because of geodesic deviation, the rays come closer together as the wave packet moves forward. They are focused. In particular the direction θ, of a ray (geodesic) with initial separation ξ after a distance r is (assuming small angles)

$$\theta = -\frac{r\xi}{R^2},$$

where R is the radius of curvature.

Since the central geodesic is the direction of energy flow, we can integrate the wave-energy-function times the component of θ normal to the trajectory, over the dimensions of the wave packet in order to calculate the amount of energy that is now traveling normal to the trajectory. The result is a finite energy that depends on the average lateral extension of the wave packet, the local radius of curvature, and the original photon energy.

The actual value is not important but rather the fact that there is a finite fraction of the energy that is moving away from the trajectory of the original wave packet. This suggests a photon interaction in which the photon interacts with curved space-time with the hypothesis that the energy flow normal to the trajectory goes into the emission of secondary photons normal to its trajectory.

From a quantum-mechanical point of view, there is a strong argument that some interaction must take place. If the spin of the photon is directly related to the angular momentum of the wave packet about its trajectory then the computation of the angular momentum is a similar integral.

Then because of *focussing* the angular momentum clearly changes along the trajectory, which disagrees with the quantum requirement that the angular momentum, that is the spin, of the photon is constant. The Heisenberg uncertainty principle requires that an incorrect value of spin can only be tolerated for a small time before something happens to restore the correct value. We now consider the consequences.

Consider motion on the surface of a three-dimensional sphere with radius r. As described above, two adjacent geodesics will move closer together due to focusing. Simple kinematics tells us that a body with velocity v asso-

ciated with these geodesics has acceleration v^2/r, where r is the radius of curvature. This acceleration is directly experienced by the body.

The geometry of a three-dimensional "surface" with curvature in the fourth dimension is essentially the same as motion in three dimensions except that the focusing now applies to the cross-sectional area and not to the separation.

Since wave packet that is subject to focusing has acceleration in an orthogonal dimension will also experience an acceleration of c^2/r normal to the surface of the sphere. Then a wave packet (and hence a photon) that has its cross-sectional area focused by curvature in the fourth dimension with radius r would have an energy loss rate proportional to this acceleration. The essence of the Curvature-redshift hypothesis is that the focusing causes the photon to interact and that the energy loss rate is proportional to c^2/R. For a photon with energy E the loss rate per unit time is cE/R, and per unit distance it is E/R.

In general relativity the crucial equation for the focusing of a bundle of geodesics was derived by Raychaudhuri (1955), also see Misner et al. (1973) and Ellis (1984) and for the current context we can assume that the bundle has zero shear and zero vorticity. Since any change in geodesic deviation along the trajectory will not alter the direction of the geodesics, we need consider only the cross-sectional area A of the geodesic bundle to get the equation

$$\frac{1}{A}\frac{d^2A}{dr^2} = -\mathbf{R}_{\alpha\beta}\mathbf{U}^\alpha\mathbf{U}^\beta = -\frac{1}{R^2}, \tag{9}$$

where $\mathbf{R}$ is the Ricci tensor (it is the contraction of the Riemann-Christoffel tensor), $\mathbf{U}$ is the 4-velocity of the reference geodesic and R is the local radius of curvature. This focusing can be interpreted as the second order rate of change of cross-sectional area of a geodesic bundle that is on the three-dimensional surface in four-dimensional space. Then if we consider that a photon is a wave packet we find that the rate at which the photon loses energy per unit distance is E/R or more explicitly.

$$\frac{1}{E}\frac{dE}{dr} = -\frac{1}{R} = -\left(\mathbf{R}_{\alpha\beta}\mathbf{U}^\alpha\mathbf{U}^\beta\right)^{1/2}, \tag{10}$$

What is interesting about this equation is that, for the Schwarzschild (and Kerr) solutions for the external field for a mass, the Ricci tensor is zero; hence, there is no focusing and no energy loss. A geodesic bundle passing a mass such as the sun experiences a distortion but the wave packet has not changed in area. Hence, this model predicts that photons passing near the limb of the sun will not suffer any energy loss due to curvature-redshift.

4.3. *Gravitation is not a force*

The phrase *gravitational force* is not only a popular expression but is endemic throughout physics. In particular, gravitation is classified as one of the four fundamental forces with its heritage going back to Newton's law of gravitation. I argue that the formulation of gravitation as a force is a misconception. In both Newtonian theory and general relativity, gravitation is acceleration. To begin let us examine the original Newtonian gravitation equation.

$$m_{\mathrm{I}}\mathbf{a} = \mathbf{F} = -\frac{GMm_{\mathrm{G}}}{r^3}\mathbf{r}, \tag{11}$$

where (following Longair (1991)) we identify m_I as the inertial mass of the test object, M as the active gravitational mass of the second object and m_{G} as the passive gravitational mass of the test object. The vector $\mathbf{a}$ is its acceleration and $\mathbf{r}$ is its displacement from the second object. This equation is usually derived in two steps: first, the derivation of a gravitational field and second, the force produced by that field on the test mass. By analogy with Coulomb's law, the passive gravitational mass has a similar role to the electric charge.

However many experiments by Eötvös, Pekár, & Fekete (1922), Dicke (1964), and Braginskij & Panov (1971) have shown that the passive gravitational mass is equal to the inertial mass to about one part in 10^{12}. The usual interpretation of the agreement is that they are fundamentally the same thing. However, an alternative viewpoint is that the basic equation is wrong and that the passive gravitational mass and the inertial mass should not appear in the equation. In this case the correct equation is

$$\mathbf{a} = -\frac{GM}{r^3}\mathbf{r}. \tag{12}$$

Thus, the effect of gravitation is to produce accelerations directly; there is no force involved. Some might argue that since the two masses cancel the distinction is unimportant. On the other hand, I would argue that the application of Ockham's razor dictates the use of Eq. 12 instead of Eq. 11.

The agreement of the inertial mass with the passive gravitational mass is the basis of the weak equivalence principle in that it applies regardless of the composition of the matter used. Carlip (1998) Shows that it applies to both the potential and the kinetic energy in the body. The theory of general relativity is based on the principle of equivalence as stated by Einstein: *All local, freely falling, non-rotating laboratories are fully equivalent for the performance of physical experiments.*

The relevance here is that it is impossible to distinguish between acceleration and a uniform gravitational

field. Thus when gravitation is considered as acceleration and not a force the passive gravitational mass is a spurious quantity that is not required by either theory.

4.4. *Derivation of Curvature-pressure.*

The hypothesis of Curvature-pressure is that for moving particles there is a pressure generated that acts back on the matter that causes the curved space-time. In this case, Curvature-pressure acts on the matter (plasma) that is producing curved space-time in such a way as to try to decrease the curvature. In other words, the plasma produces curved space-time through its density entering the stress-energy tensor in Einstein's field equations and the constraint of the plasma to a three-dimensional hyper-"surface".

A simple cosmological model using Newtonian physics in four-dimensional space illustrates some of the basic physics subsequently used to derive the features of Curvature-pressure. The model assumes that the universe is composed of plasma confined to the three-dimensional "surface" of a four-dimensional hyper-sphere.

Since the visualization of four dimensions is difficult let us suppress one of the normal dimensions and consider the gas to occupy the two-dimensional surface of a normal sphere. From Gauss's law (i.e. the gravitational effect of a spherical distribution of particles with radial symmetry is identical to that of a point mass equal in value to the total mass situated at the center of symmetry) the gravitational acceleration at the radius r of the surface is normal to the surface, directed inward and it has the magnitude

$$\ddot{r} = -\frac{GM}{r^2},\tag{13}$$

where M is the total mass of the particles and the dots denote a time derivative. For equilibrium, and assuming all the particles have the same mass and velocity we can equate the radial acceleration to the gravitational acceleration and get the simple equation from celestial mechanics of

$$\frac{v^2}{r} = \frac{GM}{r^2}.$$

If there is conservation of energy, this stable situation is directly analogous to the motion of a planet about the sun.

When there is a mixture of particles with different masses, there is an apparent problem. In general, particles will have a distribution of velocities and the heavier ones can be expected to have, on average, lower velocities. Thus, equilibrium radii will vary with the velocity of the particles.

However, the basis of this model is that all particles are constrained to have the same radius regardless of their mass or velocity with the value of the radius set by the average radial acceleration. Thus for identical particles with a distribution of velocities we average over the squared velocities to get

$$\left\langle v^2 \right\rangle = \frac{GM}{r}.\tag{14}$$

If there is more than one type of particle with different masses then we invoke the precepts of Section 4.3 and average over the accelerations to get the same result. The effect of this balancing of the accelerations against the gravitational potential is seen within the shell as a Curvature-pressure that is a direct consequence of the geometric constraint of confining the particles to a shell.

If the radius r decreases then there is an increase in this Curvature-pressure that attempts to increase the surface area by increasing the radius. For a small change in radius in a quasi-equilibrium process where the particle velocities do not change the work done by this Curvature-pressure (two dimensions) with an incremental increase of area dA is $p_c dA$ and this must equal the gravitational force times the change in distance to give

$$p_c dA = \frac{GM^2}{r^2}\,dr,$$

where $M = \sum m_i$ with the sum going over all the particles and the negative sign shows that it is opposite in effect to thermodynamic pressure. Therefore, using Eq. 14 we can rewrite the previous equation in terms of the velocities as

$$p_c dA = \frac{M\left\langle v^2 \right\rangle}{r}\,dr.$$

Now $dA/dr = 2A/r$, hence the two-dimensional Curvature-pressure is

$$p_c = \frac{M\left\langle v^2 \right\rangle}{2A}.$$

This simple Newtonian model provides a guide as to what the Curvature-pressure would be in the full general relativistic model.

In deriving a more general model in analogy to the Newtonian one, we first change $dA/dr = 2A/r$ to $dV/dr = 3V/r$ (where V is the volume) and secondly we include the correction γ^2 needed for relativistic velocities which refers to the dominant massive particles. The result is

$$p_c = \frac{\left\langle \beta^2 \right\rangle Mc^2}{3V} = \frac{\left\langle \gamma^2 - 1 \right\rangle Mc^2}{3V}.\tag{15}$$

Note that the 3 is the number of degrees of freedom. In this case the constraint arises from the confinement of all the particles within a three-dimensional hyper-"surface". Now we expect to be dealing with fully ionized high temperature plasma with a mixture of electrons, protons, and heavier ions where the averaging is done over the accelerations. Define the average density by $\rho = M/V$ then the cosmological Curvature-pressure is

$$p_c = \frac{1}{3} \left\langle 1 - \gamma^2 \right\rangle \rho c^2. \tag{16}$$

In effect, my hypothesis is that the cosmological model must include this Curvature-pressure as well as thermodynamic pressure. Note that although this has a similar form to thermodynamic pressure it is quite different. In particular, it is proportional to an average over the squared velocities and the thermodynamic pressure is proportional to an average over the kinetic energies. This means that, for plasma with free electrons and approximate thermodynamic equilibrium, the electrons will dominate the average due to their much larger velocities. From a Newtonian point of view, Curvature-pressure is opposed to gravitational mutual acceleration.

In general relativity, the plasma produces curved space-time through its density entering the stress-energy tensor in Einstein's field equations. Then the constraint of confining the particles to a three-dimensional shell produces a pressure whose reaction is the Curvature-pressure acting to decrease the magnitude of the curvature and hence decrease the density of the plasma.

4.5. The Curvature-cosmological model

Curvature-cosmology can now be derived by including Curvature-redshift and Curvature-pressure into the equations of general relativity. This is done by using homogeneous isotropic plasma as a model for the real universe. The general theory of relativity enters through the Friedmann equations for a homogeneous isotropic gas.

Although such a model is simple compared to the real universe, the important characteristics of Curvature-cosmology can be derived by using this model. The first step is to obtain the basic relationship between the density of the gas and the radius of the universe. The inclusion of Curvature-pressure is not only important in determining the basic equations but it also provides the necessary means of making the solution static and stable.

Then it is shown that the effect of Curvature-redshift is to produce a redshift that is a function of distance, and the slope of this relationship is the Hubble equation.

The first-order model considers the universe to be a gas with uniform density and complications such as density fluctuations, galaxies, and stars are ignored. In addition, we assume (to be verified later) that the gas is at high temperature and is fully ionized plasma. Because of the high symmetry, the appropriate metric is the one that satisfies the equations of general relativity for a homogeneous, isotropic gas.

Based on the Robertson-Walker metric, the Friedmann equations for the homogeneous isotropic model with constant density and pressure without the cosmological constant and with $k = 1$ are (Longair 1991)

$$\dot{R}^2 = \frac{8\pi G \rho_0}{3} R^2 - c^2 \tag{17}$$
$$\ddot{R} = -\frac{4\pi G}{3} \left(\rho + \frac{3p}{c^2} \right) R,$$

where R is the radius, ρ is the density, p is the thermodynamic pressure, G is the Newtonian gravitational constant and the superscript dots denote time derivatives.

Assuming that the thermodynamic pressure is negligible and including the Curvature-pressure, Eq. 16, the modified second Friedmann equation is

$$\ddot{R} = -\frac{4\pi G \rho}{3} \left[1 + \left\langle 1 - \gamma^2 \right\rangle \right] R, \tag{18}$$

Clearly, there is a static solution with $\ddot{R} = 0$ which means that $\gamma^2 = 2$.

The first Friedmann equation provides the radius of the universe, R_0, which is

$$R_0 = \sqrt{\frac{3c^2}{8\pi G \rho_0}} \ \text{m}, \tag{19}$$
$$= 1.268 \times 10^{13} / \sqrt{\rho_0} \ \text{m},$$
$$= 3.112 \times 10^{26} / \sqrt{N_H} \ \text{m},$$
$$= 1.008 \times 10^{4} / \sqrt{N_H} \ \text{Mpc},$$

where N_H is the number density measured in number of hydrogen atoms per m^3.

The basic instability of the static Einstein model is well known (Tolman 1934; Ellis 1984). On the other hand, the effect of Curvature-pressure is opposite in effect to the normal pressure thus Curvature-cosmology is intrinsically stable.

Now the apparent "velocity", $v(z)$ is the rate of change of z and by definition $dr/dt = c$, thus

$$v(z) = \frac{dz}{dt} = c\frac{dz}{dr} = \frac{c(1+z)}{R_0}. \tag{20}$$

Since Hubble's equation is equal to this velocity it is

$$H(z) = \frac{c(1+z)}{R_0}, \tag{21}$$

and Hubble's constant is $H_0 = c/r$ and has the value

$$H_0 = c/R_0, \text{ s}^{-1}, \qquad (22)$$
$$= 2.364 \times 10^{-5} \sqrt{\rho} \text{ s}^{-1},$$
$$= 9.6352 \times 10^{-19} \sqrt{N_H} \text{ s}^{-1},$$
$$= 29.73 \sqrt{N_H} \text{ kms}^{-1}\text{Mpc}^{-1},$$
$$= 41.30 \text{ kms}^{-1}\text{Mpc}^{-1},$$

where the last line has used $N_H = 1.93$ from section 5.2.

Since $E = ch/\lambda$ and with the redshift and using Eq. 10 provides an important equation which shows the relationship between the cosmic distance and redshift and is

$$\frac{1}{E}\frac{dE}{dr} = -\frac{1}{R_0}, \qquad (23)$$

Thus the energy loss for this cosmic distance is

$$\log(E(r)/E_0) = -r/R_0. \qquad (24)$$

Since $z = (\lambda/\lambda_0 - 1)$ and $E = ch/\lambda$ then

$$r = R\log(1 + z). \qquad (25)$$

With a constant density, integration provides an alternative form for the redshift which is

$$z = \exp(-r/R) - 1. \qquad (26)$$

Since Eq. 23 is valid for any function of time it means that the Type Ia supernova light curve must have a $(1+z)$ width dependence.

Of interest is that the distance to the furthest point is $r/R = \pi$ which has a redshift of $z = 22.141$. The light travel time to that point is $\pi R_0 c = 7.439 \times 10^{10}$ years.

If there is a region in the cosmic plasma that has a different density then the effective universe radius, R, is provided by Eq.19 with the energy loss given by Eq. 24.

The total volume of the universe is $2\pi^2 R_0^3 = 2.22 \times 10^{80}$ m^3. Thus there are a total of 4.286×10^{80} hydrogen atoms with a mass of 7.13×10^{53}kg.

4.6. *Distance modulus.*

The geometry of Curvature-cosmology is that of a three-dimensional "surface" of a four-dimensional hyper-sphere with radius R_0. For this geometry the area is

$$A(r) = 4\pi[R\sin(r/R_0)]^2.$$

Let a source have a luminosity $L(\nu)$ (W Hz^{-1}) at the emission frequency ν. Then if energy is conserved, the observed flux density, $F(\nu)$ (W m^{-2} Hz^{-1}) at a distance parameter z is the luminosity divided by the area, which is

$$F(\nu)d\nu = \frac{L(\nu)\,d\nu}{4\pi[R\sin(r/R_0)]^2}.$$

However, because of Curvature-redshift there is an energy loss that is proportional to $(1+z)$. The total energy loss is equivalent to an integral of the incremental energy loss as a function of r. But what is required is the total energy loss as a function of z. Since $dr/dz = 1/(1 + z)$ this will cancel the intrinsic energy loss to provide

$$F(\nu_0)d\nu_0 = \frac{L(\nu_0)\,d\nu_0}{4\pi[R_0\sin(\log(1 + z))]^2}.$$

Since the absolute magnitude is the apparent magnitude when the object is at a distance of 10 pc then

$$F_{10}(\nu_0)\,d\nu_0 = \frac{1}{10pc/R_0},$$

where because 10 pc is negligible compared to R, approximations have been made. The flux density ratio is

$$F(\nu_0) = \left[\frac{10pc/R_0}{\sin(\log(1 + z))}\right]^2.$$

The apparent magnitude is defined as $m = -2.5\log(S)$ where the base of the logarithm is 10 and the constant 2.5 is exact and M as the absolute magnitude we get the distance modulus, $\mu = m - M$ to be

$$\mu = 5\log_{10}[\sin(\log(1 + z))] + 44.304. \qquad (27)$$

4.7. *Temperature of the cosmic plasma*

One of the most remarkable results of Curvature cosmology is that it predicts the temperature of the cosmic plasma from fundamental constants. That is the predicted temperature is only dependent on the electron density of the intra-galactic medium.

For a stable solution to Eq. 18 we need that $<\gamma^2> = 2$, where the average (denoted by $(< >)$) is taken over the proton number densities. Since the total energy for a particle is γmc^2 the kinetic energy is $E(\gamma - 1)mc^2$. In this case for protons $E = 3.391E^{-14}$ J and from $E = kT$ the plasma temperature is

$$T = 2.456E9 \text{ K}. \qquad (28)$$

4.8. *Black holes and Jets*

Consider a very small homogeneous mass with a radius R. Its dynamics are described by the Friedmann equations Eq. 17, and if the acceleration is zero then $\dot{R}_B = 0$ and

$$\frac{8\pi G\rho_0 R_1^2}{3} = c^2,$$

and substituting for the density $\rho_0 = 3m/(4\pi R_1^3)$, the radius is

$$R_B = \frac{2Gm}{c^2}. \qquad (29)$$

14

This is the Schwarzschild radius for a simple theoretical black hole,.

Since the acceleration is zero, it is an absolute minimum radius and smaller radii are inaccessible. This object has all the external properties of a black hole, such as accretion disks. Thus it looks like the theoretical black hole but is not a black hole.

Since the radii smaller that R_B are inaccessible there is no problem with the divergence of space time at zero radius which may help the understanding of quantum gravity.

If the compact object is rotating there is the tantalizing idea that Curvature-pressure may produce the emission of material in two jets parallel to the spin axis. The limiting distance will be determined by the polar radius. Thus radii greater than this, such as the equatorial radii will still be able to emit energy that can be seen. Thus the object will appear like a doughnut with zero radiation at the center and with a very broad jet parallel to the spin axis.

This could be the 'jet engine' that produces the astrophysical jets seen in stellar-like objects and in many huge galactic radio sources. More importantly it acts to recycle its mass to the cosmic plasma.

4.9. *Inhibition of Curvature-redshift*

from the discussion above it is clear that the process of Curvature-redshift requires a gradual focusing to a critical limit, followed by the emission of secondary photons. It is as if the photon gets slowly excited by the focusing until the probability of secondary emission becomes large enough for it to occur.

If there is any other interaction the excitation due to focusing will be nullified. That is, roughly speaking, Curvature-redshift interaction requires an undisturbed path length of at least $\lambda_{secondary}$ for the interaction to occur. Thus suitable criterion for inhibition to occur is that the competing interaction has an interaction length less than $\lambda_{secondary}$

Although Compton or Thompson scattering are possible inhibitors, there is another interaction that has a much larger cross-section. This is the coherent multiple scattering that produces refractive index.

In classical electromagnetic theory, the refractive index of a medium is the ratio of the velocity of light in vacuum to the group velocity in the medium. However, in quantum mechanics photons always travel at the velocity of light in vacuum. In a medium, a group of photons appears to have a slower velocity because the individual photons interact with the electrons in the medium and each interaction produces a time delay.

Because the interaction of a photon is with many electrons spread over a finite volume, the only possible result of each interaction is the emission of another photon with the same energy and momentum. Now consider the absorption of a wave. In order to cancel the incoming wave a new wave with the same frequency and amplitude but with opposite phase must be produced. Thus, the outgoing wave will be delayed by half a period with respect to the incoming wave. If the phase difference was not exactly half a period for an electromagnetic wave incident on many electrons, the principle of conservation of energy would be violated.

This simple observation enables us to compute the interaction length for refractive index n. If L is this interaction length then it is

$$L = \frac{\lambda_0}{2\,|n-1|},$$

where n is the refractive index and the modulus allows for plasma and other materials where the refractive index is less than zero.

Note that L is closely related to the extinction length derived by Ewald and Oseen (see (Jackson 1975) or Born & Wolf (1999)) which is a measure of the distance needed for an incident electromagnetic wave with velocity c to be replaced by a new wave.

For plasmas the refractive index is

$$n \cong 1 - \frac{N_H \lambda_0^2}{2\pi r_0},$$

where N_H is the electron density and r_0 is the classical electron radius. We can combine these two equations to get (for a plasma)

$$L = (N_H r_0 \lambda_0)^{-1}. \tag{30}$$

Thus, we would expect the energy loss to be inhibited if the average Curvature-redshift interaction distance is greater than that for refractive-index interactions. Therefore, we can compute the ratio (assuming a plasma with $N \cong N_H$) to get

$$\lambda_{secondary}/L = 0.0106 N_H^{3/4} \lambda_0^{3/2} \tag{31}$$

This result shows that Curvature-redshift will be inhibited if this ratio is greater than one, which is equivalent to $\lambda_0 \geq 20.7 N_H^{-1/2}$ m. For example, Curvature-redshift for the 21 cm hydrogen line will be inhibited if the electron density is greater than about $10^4\,\mathrm{m}^{-3}$.

4.10. *Possible laboratory tests.*

It is apparent from the above analysis that to observe the redshift in the laboratory we need to have sufficient

density of gas (or plasma) to achieve a measurable effect but not enough for there to be inhibition by the refractive index.

The obvious experiment is to use the Mössbauer effect for γ-rays that enable very precise measurement of their frequency. Simply put, the rays are emitted by nuclei in solids where there is minimal recoil or thermal broadening of the emitted ray.

Since the recoil momentum of the nucleus is large compared to the atomic thermal energies and since the nucleus is locked into the solid so that the recoil momentum is precisely defined, then the γ-ray energy is also precisely defined. The absorption process is similar and has a very narrow line width.

Such an experiment has already been done by Pound & Snider (1965). They measured gravitational effects on 14.4 keV γ-rays from ^{57}Fe being sent up and down a vertical path of 22.5m in helium near room pressure. They found agreement to about 1% with the predicted fractional redshift of 1.5×10^{-15}, whereas fractional Curvature-redshift predicted by Eq. 10 for this density is 1.25×10^{-12}. Clearly, this is much larger.

At γ-ray frequencies, the electrons in the helium gas are effectively free and we can use Eq. 30 to compute the refractive index interaction length. For helium at STP, it is $L = 0.077$ m, which is much less than Curvature-redshift interaction length which for these conditions is $X=11$ m. Hence, we do not expect to see any significant Curvature-redshift in their results.

Pound and Snyder did observe one-way frequency shifts but they were much smaller than Curvature-redshift and could be explained by other aspects of the experiment. However, the Pound and Snyder experiment provide a guide to a possible test for the existence of Curvature-redshift. Because Curvature-redshift has a different density variation to that for the inhibiting refractive index it is possible to find a density for which Curvature-redshift is not inhibited.

Although there is a slight advantage in using heavier gases than helium due to their higher atomic number to atomic weight ratio, their increased absorption to γ-rays rules them out. Hence, we stay with helium and from Eq. 30 we can compute Curvature-redshift interaction length to be

$$X = 10.8 \left(\frac{p_0}{p} \right)^{1/4} \text{ m},$$

where p is the pressure and p_0 is the pressure at STP. For the same gas the refractive-index interaction length is

$$L = 0.077 \left(\frac{p_0}{p} \right) \text{ m}.$$

It follows that the Curvature-redshift will not be inhibited if $X < L$ or in this case, the pressure is less than $0.0014 p_0$ which is about 1 mm of Hg. For this pressure, we find that $X = 57$ m which requires that the apparatus must be much longer than 57 m. For argument let us take the length to be 100 m then the fractional redshift expected is 2.1×10^{-13} which is detectable.

The experimental method would use a horizontal (to eliminate gravitational redshifts) tube filled with helium and with accurately controlled temperature. Then we would measure the redshift as a function of pressure. The above theory predicts that if it is free of inhibition then the redshift should be proportional to the square root of the pressure.

Alternatively, it may be possible to detect the secondary photons. For helium with a pressure of 1 mm Hg the expected frequency of the secondary radiation from ^{57}Fe is about 100 kHz. The expected power from a 1 Cu source is about 5×10^{-22} W. Unfortunately, the secondary radiation could be spread over a fairly wide frequency band which makes its detection somewhat difficult but it may be possible to detect the radiation with modulation techniques.

5. PART C: OBSERVATIONS

5.1. *Type Ia supernova*

For the 1,652 Type Ia supernova analyzed in Part A the light curve width is

$$w_{obs}(z) = 1.060 \pm 0.009 + (1.080 \pm 0.042)\, z, \qquad (32)$$

which shows an excellent agreement with the expected $(1 + z)$ width dependence.

The distribution of the apparent magnitudes is shown in Figure 4. and the regression of the absolute magnitude using Eq. 27, as a function of redshift for Curvature-cosmology is

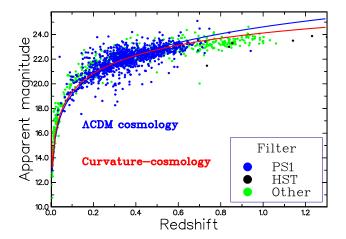$$M(z) = -20.446 \pm 0.012 - (0.081 \pm 0.057)\, z,$$

which also shows excellent agreement with a constant value.

However as shown in section 3.7 the regression for the 1652 Type Ia supernova, using the intrinsic analysis and the oCDM model, is

$$M(z) = -18,562 \pm 0.009 + (0.669 \pm 0.059)z. \qquad (33)$$

It was argued there that this is because of a fault in the SALT2 analysis.

In the standard model, this result is said to be the consequence of dark energy that increases the apparent velocity at large redshifts. For this set of Type Ia supernova, the apparent velocity is $(1+z)+(0.697\pm0.064)z^2$. A plot of their absolute magnitudes is shown in Figure 5.

Figure 4. The cosmological apparent magnitude of the current Type Ia supernova as a function of redshift. The blue curve is the distance modulus for the oCDM model. The red curve is the distance modulus for Curvature-cosmology.
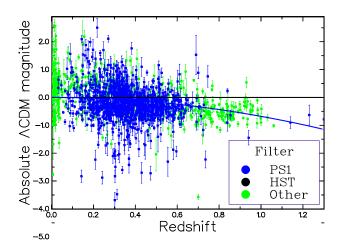

Figure 5. The absolute magnitude of the current Type Ia supernova as a function of redshift for the oCDM model. The blue curve shows the dark energy magnitude change of $(0.697 \pm 0.064)z^2$.

5.2. X-ray background radiation

Since Giacconi et al. (1962) observed the X-ray background there have been many suggestions made to explain its characteristics. Although much of the unresolved X-ray emission comes from active galaxies, there is a part of the spectrum between about 10 keV and 1 MeV that is not adequately explained by emission from discrete sources. The very high energy range is most likely due to external point sources. It is the intermediate range that is examined here.

In ΛCDM cosmology for the intermediate X-ray range of about 10–300 keV, the production of X-rays in hot cosmic plasma through the process of bremsstrahlung

has been suggested by Hoyle (1962); Gould & Burbidge (1963); Field & Henry (1964); Cowsik & Kobetich (1972).

In a review of the spectrum of the X-ray background radiation Holt (1992) concluded that the measured spectra of discrete sources are not consistent with the observations in the intermediate energy range but there is a remarkable fit to a 40 keV $(4.6 \times 10^8$ K) bremsstrahlung spectrum from a diffuse hot gas.

However, in an expanding universe most of the X-rays are produced at redshifts of $z \approx 3$ where the density is large enough to scatter the CMBR. This scattering known as the Sunyaev–Zel'dovich effect (see Section 5.12) makes a distinct change in the spectrum of the CMBR. This predicted change in the spectrum has not been observed and this is the major reason why the bremsstrahlung model in ΛCDM is rejected.

In Curvature-cosmology, the basic component of the universe is plasma with a very high temperature, and with low enough density to avoid the Sunyaev–Zel'dovich effect.

The background X-ray emission is produced in this plasma by the process of free-free emission (bremsstrahlung). The observations of the background X-ray emission are analyzed in order to measure the density and temperature of the plasma. In Curvature-cosmology, this density is the major free parameter and it determines the size of the universe and the value of the Hubble constant.

In addition, the temperature of the plasma determined from the X-ray measurements can be compared with the predicted value from Curvature-cosmology for pure hydrogen of 2.456×10^9 K.

The first step is to calculate the expected X-ray emission from high temperature plasma in thermal equilibrium. Here the dominant mechanism is bremsstrahlung radiation from electron-ion and electron-electron collisions. With a temperature T and emission into the frequency range ν to $\nu + d\nu$ the volume emissivity per steradian can be written as

$$j_\nu(\nu)d\nu = \left(\frac{16}{3}\right)\left(\frac{\pi}{6}\right)^{1/2} r_0^3 m_e c^2 \left(\frac{m_e c^2}{kT}\right)^{1/2}$$
$$\times g(\nu, T) \exp\left(-\frac{h\nu}{kT}\right) N_H \sum Z_i^2 N_i \, d\nu \quad (34)$$

where $g(\nu, T)$ is the Gaunt factor, N_H is the electron number density, N_i is the ion number density and r_0 is the classical electron radius and the other symbols have their usual significance (Nozawa, Itoh, & Kohyama 1998). The intensity, $j_\nu(\nu)$, has the units of $W\,m^{-3}\,Hz^{-1}$.

As it stands this equation does not include the electron-electron contribution. Nozawa et al. (1998) and Itoh et al. (2000) have done accurate calculations for many light elements. Based on their calculations Professor Naoki Itoh (http://www.ph.sophia.ac.jp/) provides a subroutine to calculate the Gaunt factor that is accurate for temperatures greater than 3×10^8 K. It is used here.

Because of the very high temperature, we can assume that all atoms are completely ionized. Thus, Eq. 34 including the Gaunt factor provides the production rate of X-ray photons as a function of the plasma temperature and density.

The next step is to compute the expected intensity at an X-ray detector. Consider an X-ray photon that is produced at a distance r from the detector. During its travel to the detector, it will have many Curvature-redshift interactions. Although the photon is destroyed in each interaction, there is a secondary photon produced that has the same direction but with a slightly reduced energy.

It is convenient to consider this sequence of photons as a single particle and to refer to it as a primary photon. The important result is that the number of these primary photons is conserved. Therefore, we need the production distribution of the number of photons per unit energy interval. The number of photons emitted per unit volume per unit time in the energy interval ε to $\varepsilon + d\varepsilon$ is given by

$$j_n(\varepsilon)\, d\varepsilon = \frac{j_\nu(\nu)}{\varepsilon} h\, d\nu, \tag{35}$$

where $\varepsilon = h\nu$, h is Plank's constant and $j_\nu(\nu)$ is the energy distribution per unit frequency interval.

Now consider the contribution to the number of X-rays observed by a detector with unit area. Because the universe is static, the area at a distance r from the source is the same as the area at a distance r from the detector. Since there is conservation of these photons, the number coming from a shell at radius r per unit time and per steradian within the energy interval ε to $\varepsilon + d\varepsilon$ is

$$\frac{dn(r)}{dt}\, d\varepsilon = j_n(\varepsilon) d\varepsilon r\, d\chi.$$

Next, we integrate the photon rate per unit area and per steradian from each shell where the emission energy is ε and the received energy is ε_0 to get

$$I_n(\varepsilon_0)\, d\varepsilon_0 = r \int_0^{\chi_m} j_n(\varepsilon)\, d\varepsilon\, d\chi,$$

where $\varepsilon = (1 + z)\varepsilon_0$ and it is assumed that the flux is uniform over the 4π steradian. Furthermore, it is useful to change the independent coordinate to the redshift parameter z.

Then using Eq. 35 we get

$$I_\nu(\nu_0)\, d\nu_0 = \frac{c}{H} \int_0^{z_m} \frac{j_\nu(\nu)}{1+z}\, dz\, d\nu_0,$$

where H is the Hubble constant and the change in bandwidth factor $d\nu/d\nu_o$, cancels the $(1+z)$ factor that comes from the change in variable from $d\chi$ to dz but there is another divisor of $(1 + z)$ that accounts for the energy lost by each photon.

Thus the energy flux per unit area, per unit energy interval, per unit frequency and per solid angle is given by Eq. 36 where Plank's constant is included to change the differential from frequency to energy. The z_m limit of 8.2 comes from the limit of $\chi \leq \pi$.

$$\begin{aligned}
I_\nu &= \left(\frac{16}{3}\right)\left(\frac{\pi}{6}\right)^{1/2} \frac{r_0^3 m_e c^3}{h} \left(8\pi G M_H\right)^{-1/2} \left(\frac{mc^2}{kT}\right)^{1/2} \\
&= \times n_e n_i N_H^{3/2} \int_0^{z_m} \frac{g\left((1+z)\nu_0, T\right)}{(1+z)} \exp\left(-\frac{h(1+z)\nu_0}{kT}\right) dz \\
&= \frac{1.9094 \times 10^3\, \mathrm{keV}}{\mathrm{keV\, m^2\, s\, sr}} \left(\frac{mc^2}{kT}\right)^{1/2} n_e n_i N_H^{3/2} \\
&\quad \times \varepsilon_0 \int_0^{z_m} \frac{g\left((1+z)\nu_0, T\right)}{(1+z)} \exp\left(-\frac{h(1+z)\nu_0}{kT}\right) dz, \quad (36)
\end{aligned}$$

where I_ν is a function of ν_0.

The density N_H is obtained by fitting Eq. 36 to the observed data as a function of the temperature T, and then extracting N_H from the normalization constant.

The X-ray data used is tabulated in Table 4. It consists of the background X-ray data cited in the literature and assessed as being the latest or more accurate results. Preliminary analysis showed that there were some discrepant data points that are listed in Table 5 in order of exclusion.

Very hard X-rays cannot be produced even by this hot plasma and are presumably due to discrete sources (Holt 1992).

The results of the fit of the data to this model of pure hydrogen is a temperature of

$$(2.62 \pm 0.13) \times 10^9\, \mathrm{K}, \tag{37}$$

which is good agreement with the predicted temperature of 2.456×10^9 K.
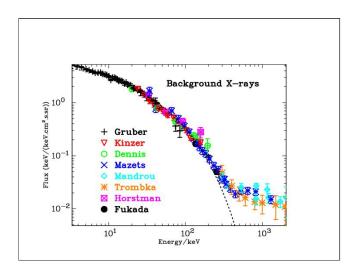
The measured density is

$$1.93 \pm 0.13\, \mathrm{H\ atoms\ per\ m^3}, \tag{38}$$

Table 4. List of background X-ray data used.

Name	Instrument	Reference
Gruber	HEAO 1 A-4	Gruber et al. (1999)
Kinzer	HEAO 1 MED	Kinzer et al. (1997)
Dennis	OSO-5	Dennis et al. (1973)
Mazets	Kosmos 541	Mazets et al. (1975)
Mandrou	Balloon	Mandrou et al. (1979)
Trombka	Apollo 16, 17	Trombka et al. (1977)
Santalogo	Rocket	Santangelo et al. (1973)
Fukada	Rocket	Fukada et al. (1975)

Table 5. Background X-ray data: rejected points.

Source	Energy	Flux density	χ^2
	keV	keV/(keV cm^2 s sr)	(1 DoF)
Gruber	98.8	0.230±0.012	108.6
Gruber	119.6	0.216±0.022	65.2
Fukada	110.5	0.219±0.011	66.6
Gruber	152.6	0.140±0.022	50.9
Fukada	179.8	0.110±0.005	41.5
Gruber	63.9	0.484±0.034	25.1

Figure 6. Background X-ray spectrum. See Table 4 for list of observations. The dashed (black) line is best fit from 10 keV to 300 keV for the pure hydrogen model.

which is the only free parameter in Curvature-cosmology.

Most of the X-ray flux below 10 keV and part of the flux just above 10 keV is emission from discrete sources. The deviation from the curve at energies above about 300 keV arises from X-rays coming from discrete sources.

In the intermediate region where bremsstrahlung should dominate, there are clear signs of some minor systematic errors. In addition, there appears to be some variation between the data sets. It is not clear whether the discrepancy between the observed points and the predicted flux densities is due to an inadequate theory, inadequate X-ray emission model, or systematic errors in the observations. After all the measurements are very difficult and come from a wide range of rocket, balloon and satellite experiments. In particular, the recent HEAO results Kinzer et al. (1997) differ from earlier results reported by Marshall et al. (1980).

5.3. *Cosmic microwave background radiation.*

The cosmic microwave background radiation (CMBR) is one of the major success stories for the standard model. The observed radiation has a spectrum that is extremely close to a black body spectrum which means that it can be described by a single parameter, its temperature.

Observations of the CMBR spectrum were obtained from the FIRAS instrument on the *Cobe* satellite by Mather et al. (1990). They measured the temperature of the CMBR to be 2.725 K. This temperature is in agreement with the observations of Roth & Meyer (1995) who measured a temperature of $2.729(+0.023, -0.031)$ K using cyanogen excitation in diffuse interstellar clouds. More recently Fixsen (2009) using data from the Wilkinson Microwave Anisotropy Probe (WMAP) and many earlier results provide a temperature of 2.72548 ± 0.00057K.

Since electrons and nucleons have wave properties they are subject to Curvature-redshift where the basic energy loss is $\Delta E = E_0 r/R$, where E_0 is the particle energy and r is the distance traveled. With a velocity of βc the distance traveled is $r = \beta c t$ and the rate of energy loss is

$$\frac{\Delta E}{dt} = \frac{E_0 \beta c}{R_0}. \qquad (39)$$

The distribution of relativistic particles in equilibrium is the Maxwell-Jüttner distribution. With $\gamma = 1/\sqrt{1 - v^2/c^2}$ it is

$$f(\gamma) = \frac{\gamma^2 \beta}{\theta K_2(1/\theta)} \exp(-\gamma/\theta), \qquad (40)$$

where $\theta = kT/mc^2$ and K_2 is the modified Bessel function of the second kind.

Here its application requires that θ is a constant value, $\theta = \sqrt(2$, then the integral over the range of γ is

$$\frac{\Delta E}{dt} = \frac{\gamma^2 \beta^2 c(\gamma - 1) m_p c^2}{R_0} \exp(-\gamma/\theta)/A, \qquad (41)$$

where A is the normalization constant and it is

$$A = \int_1^\infty \gamma^2 \beta (\exp(-\gamma/\theta) d\gamma. \qquad (42)$$

As explained earlier this lost energy consists of a pair of identical photons whose usual interaction with the electrons and photons bring them into thermal equilibrium. Since the total energy must be conserved, the energy lost by Curvature-redshift must be radiated by the emittance of these photons. Then allowing for the proton number density $N_H = 1.93 \pm 0.13$, section 5.2, their equilibrium temperature is 2.736 ± 0.092K. This radiation is the cosmic microwave background radiation and is within 0.4% of the WMAP value. Considering that the theory has only one free parameter, the agreement is exceptional good.

Clearly, the same analysis can be applied to the free electrons. In this case the radiation has a temperature of 0.419K with a wavelength of 34.4mm.

5.4. *Tolman surface density.*

This test, suggested by Tolman (1934), relies on the observation that the surface brightness (SB) of objects does not depend on the geometry of the universe. Although it is obviously true for Euclidean geometry, it is also true for most non-Euclidean geometries. For a uniform source, the quantity of light received per unit angular area is independent of distance. However, the quantity of light is also sensitive to non-geometric effects, which make it an excellent test to distinguish between cosmologies. For expanding universe cosmologies the surface brightness is predicted to vary as $(1 + z)^{-4}$, where one factor of $(1 + z)$ comes from the decrease in energy of each photon due to the redshift, another factor comes from the decrease in the rate of their arrival and two factors come from the apparent decrease in area due to aberration. This aberration is simply the rate of change of area for a fixed solid angle with redshift. In a static, tired-light, cosmology (such as Curvature-cosmology) only the first factor is present. Thus an appropriate test for Tolman surface brightness is the value of this exponent.

The obvious candidates for surface brightness tests are elliptic and S0 galaxies which have minimal projection effects compared to spiral galaxies . The major problem is that surface brightness measurements are intrinsically difficult due to the strong intensity gradients across their images. In a series of papers Sandage & Lubin (2001); Lubin & Sandage (2001a,b,c) (hereafter SL01) have investigated the Tolman surface brightness test for elliptical and S0 galaxies. More recently Sandage (2010) has done a more comprehensive analysis but since he came

to the same conclusion as the earlier papers and since the earlier papers are better known this analysis will concentrate on them.

The observational difficulties are thoroughly discussed by Sandage & Lubin (2001) with the conclusion that the use of Petrosian metric radii helps solve many of the problems. Petrosian (1976); Djorgovski & Spinrad (1981); Sandage & Perelmuter (1990) showed that if the ratio of the average surface brightness within a radius is equal to η times the surface brightness at that radius then that defines the Petrosian metric radius, η. The procedure is to examine an image and to vary the angular radius until the specified Petrosian radius is achieved.

Thus, the aim is to measure the mean surface brightness for each galaxy at the same value of η. The choice of Petrosian radii greatly diminishes the differences in surface brightness due to the luminosity distribution across the galaxies. However, there still is a dependence of the surface brightness on the size of the galaxy which is the Kormendy relationship (Kormendy 1977).

The purpose of the preliminary analysis done by SL01 is not only to determine the low redshift absolute luminosity but also to determine the surface brightness verses linear size relationship that can be used to correct for effects of size variation in distant galaxies. The data on the nearby galaxies used by SL01 was taken from Postman & Lauer (1995) and consists of extensive data on the brightest cluster galaxies (BCG) from 119 nearby Abell clusters. All magnitudes for these galaxies are in the R_C (Cape/Landolt) system.

Since the results for different Petrosian radii are highly correlated the analysis repeated here using similar procedures will use only the Petrosian $\eta = 2$ radius. Although the actual value used for the Hubble constant does not alter any significant results here, it is set to h=50 km s^{-1} Mpc^{-1} for numerical consistency. A minor difference is that the angular radius used here is provided by Curvature-cosmology whereas SL01 used the older Mattig equation.

The higher z data comes from SL01. They made Hubble Space Telescope observations of galaxies in three clusters and measured their surface brightness and radii. The names and redshifts of these clusters are given in Table 6 which also shows the number of galaxies in each cluster, N, the logarithm of the average metric radius in kpc, $\log(S_{BB})$, and the average apparent magnitude and the absolute magnitude. In order to avoid confusion in BB denotes a measurement made using the standard ΛCDM cosmology. Note that the original magnitudes for Cl 1324+3011 and Cl 1604+4304 were observed in the I band.

Table 6. Galactic properties for Petrosian radius $\eta = 2.0$

Cluster	N	$\overline{\log(S_{BB})}$	$\overline{m_{BB}}$	$\overline{M_{BB}}$
Nearby	74	4.69±0.28	22.56±0.84	-23.84±0.66
1324+3011	11	3.99±0.21	22.87±0.75	-23.28±0.65
1604+4304	6	4.05±0.17	22.34±0.60	-23.51±0.68
1604+4321	13	4.00±0.15	22.35±0.78	-23.33±0.64

Table 7. Fitted exponents for distant clusters ($\eta = 2.0$)

Cluster	Col	$\overline{z}$	n_{BB}	n_{SL01}
1324+3011	I	0.757	1.98±0.19	1.99±0.15
1604+4304	I	0.897	2.22±0.22	2.29±0.21
1604+4321	R	0.924	2.24±0.18	2.48±0.25

In order to get a reference surface brightness at $z = 0$ all the surface brightness values, SB, of the nearby galaxies were reduced to absolute surface brightness by using Eq. 43. Since all the redshifts are small, this reduction is essentially identical for all cosmological models. However the calculation of the metric radii for the distant galaxies is very dependent on the cosmological model.

This procedure of using the same cosmology in analyzing a test of that cosmology is discussed in SL01. Their conclusion is that it reduces the significance of a positive result from being *strongly supportive* to being *consistent with the model*. Of interest is that Table 6 shows that on average the distant galaxies are fainter than the nearby galaxies.

Then a linear least squares fit of the absolute surface brightness as a function of $\log(S_{BB})$, the Kormendy relationship, for the nearby galaxies results in the equation

$$SB = 9.29 \pm 0.50 + (2.83 \pm 0.11)\log(S_{BB}), \quad (43)$$

whereas SL01 found the slightly different equation

$$SB = 8.69 \pm 0.06 + (2.97 \pm 0.05)\log(S_{BB}). \quad (44)$$

Although a small part of the discrepancy is due to slightly different procedures, the main reason for the discrepancy is unknown. Of the 74 galaxies used, there were 19 that had extrapolated estimates for either the radius or the surface brightness or both. In addition there were only three galaxies that differed from the straight line by more than 2σ. They were A147 (2.9σ), A1016 (2.0σ)and A3565 (-2.4σ). Omission of all or some of these galaxies did not improve the agreement. The importance of this preliminary analysis is that Eq. 43 contains all the information that is needed from the nearby galaxies in order to calibrate the distant cluster galaxies.

Next we use the galaxies' radius and Eq. 43 to correct the apparent surface brightness of the distant galaxies for the Kormendy relation and then do least squares fit to the difference between the corrected surface brightness and its absolute surface brightness as a function of $2.5\log(1 + z)$ to estimate the exponent, n, where $SB \propto (1 + z)^n$. If needed the non-linear corrections

given by Sandage (2010) were applied to the nearby surface brightness values. For the I band galaxies, the absolute surface brightness included the color correction $< R - I > = 0.62$ Lubin & Sandage (2001c).

The results for the exponent, n, for each cluster are shown in Table 7 together with the values from SL01 (column 5) where the second column is the band (color) in which the cluster was observed.

Because the definition of magnitude contains a negative sign the expected value for n in BB is four. Nearly all of the difference between these results and those from SL01 arise from the use of a different Kormendy relationship. If the Kormendy relationship used by SL01 Eq. 44 is used instead of Eq. 43) the agreement is excellent. If it is assumed that there is no evolutionary or other differences between the three clusters and all the data are combined the resulting exponent is $n_{BB} = 2.16 \pm 0.13$.

Clearly, there is a highly significant disagreement between the observed exponents and the expected exponent of four. Both SL01 and Sandage (2010) claim that the difference is due to the effects of luminosity evolution. Based on a range of theoretical models SL01 show that the amount of luminosity evolution expressed as the exponent, $p = 4 - n_{BB}$, varies between $p =$0.85–2.36 in the R band and $p =$0.76–2.07 in the I band. In conclusion, to their analysis, they assert that *they have either (1) detected the evolutionary brightening directly from the SB observations on the assumption that the Tolman effect exists or (2) confirmed that the Tolman test for the reality of the expansion is positive, provided that the theoretical luminosity correction for evolution is real.*

SL01 also claims that their results are completely inconsistent with a tired light cosmology. Although this is explored for Curvature-cosmology in the next subsection, it is interesting to consider a very simple model. The essential property of a tired light model is that it does not include the time dilation factor of $(1 + z)$ in its angular radius equation. Thus assuming BB but without the $(1 + z)$ term all values of $\log(S_{BB})$ will be increased by $\log(1 + z)$. Hence the predicted absolute surface brightness will be (numerically) increased by $(2.83/2.5)\log(1 + z)$. For example, the exponent for

Table 8. Radii and fitted exponents for distant clusters ($\eta = 2.0$)

Cluster	N	$\overline{\log(S)}$	$\bar{M}$	n
nearby	74	4.70±0.28	-23.78±0.66	
1324+3011	11	4.18±0.21	-22.41±0.66	1.19±0.19
1604+4304	6	4.27±0.17	-22.54±0.65	1.45±0.21
1604+4321	13	4.23±0.15	-22.33±0.68	1.48±0.17

all clusters will be changed to

$$n_{\text{tired\_light}} = 2.16 \pm 0.16 - \frac{2.83}{2.5} = 1.03 \pm 0.16.$$

This is clearly close to the expected value of unity predicted by a tired-light cosmology and thus disagrees with the conclusion of SL01 that the data are incompatible with a tired light cosmology.

There are two major criticisms of this work. The first is that relying on theoretical models to cover a large gap between the expected index and the measured index makes the argument very weak. Although SL01 indirectly consider the effects of relatively common galaxy interactions and mergers in the very wide estimates they provide for the evolution, the fact that there is such a wide spread makes the argument that Tolman surface brightness for this data is consistent with ΛCDM possible but weak.

Ideally, there would be an independent estimate of p based on other observations. The second criticism is that the nearby galaxies are not the same as the distant cluster galaxies. The nearby galaxies are all brightest cluster galaxies (BCG) whereas the distant cluster galaxies are normal cluster galaxies. It is well known that BCG (Blanton & Moustakas 2009) are in general much brighter and larger than would be expected for the largest member of a normal cluster of galaxies. Whether or not this amounts to a significant variation is unknown but it does violate the basic rule that like should be compared with like.

Unsurprisingly it is found that using Curvature-cosmology the relationship between absolute surface brightness and radius is identical to that shown in Table 6. What is different is the average radius, the absolute magnitudes and the observed exponent n. These are shown in Table 8.

The result for all clusters is $n = 1.38 \pm 0.13$ which is in agreement with unity. Note that the critical difference from the standard analysis is in the size of the radii. They are not only much closer to the nearby galaxy radii but because they are larger they do not require the non-linear corrections for the Kormendy relation. As before

we note that the nearby galaxies are BCG which may have a brighter SB than the normal field galaxies. If this is true, it would bias the exponent to a larger value. If we assume that Curvature-cosmology is correct then this data shows that on average the BCG galaxies are -0.64 ± 0.08 mag (which is a factor of 1.8 in luminosity) brighter than the general cluster galaxies.

The SL01 data for the surface brightness of elliptic galaxies is consistent with ΛCDM but only if a large unknown effect of luminosity evolution is included. The data do not support expansion and are in complete agreement with Curvature-cosmology.

5.5. *Dark matter and Coma cluster*

All observational evidence for dark matter comes from the application of Newtonian gravitational physics to either clusters of objects or the rotation of galaxies. Galaxy rotation will be dealt with in Section 5.19. The original concept for dark matter comes from applying the virial theorem to the Coma cluster of galaxies (Zwicky 1937). The virial theorem is a statistical theorem that states that for an inverse square law the average kinetic energy of a bound system is equal to half the potential energy (i.e. $2T + V = 0$).

Then with knowing the linear size of the cluster and measuring the mean square spread of velocities we can estimate the total mass of the cluster. There is no doubt that applying the virial theorem to the Coma and other clusters of galaxies provides mass estimates that can be several hundred times the mass expected from the total luminosity. Even the mass of intergalactic gas is not enough to overcome this imbalance. In ΛCDM cosmology dark matter has been introduced to make up for the shortfall of mass.

However if Curvature-cosmology is valid then it is possible that the observed redshifts are not due to kinematic velocities but are Curvature-redshifts produced by the intergalactic gas. The purpose of this section is to show that Curvature-redshift can explain the galactic velocities without requiring dark matter.

For simplicity, we will use the Coma cluster as a test bed. Not only is it very well studied, but it also has a high degree of symmetry and the presence of an intergalactic gas cloud is known from X-ray observations. Watt et al. (1992) and Hughes (1989) have fitted the density of the gas cloud to an isothermal model with the form

$$\rho = \rho_0 \left(1 + \left(\frac{r}{r_e} \right) \right)^{-\alpha}, \qquad (45)$$

with a center at $12^h 59^m 10^s, 27°59'56''$ (J2000) and with $r_e = 8.8' \pm 0.7'$, $\alpha = 1.37 \pm 0.09$, $\rho_0 = (2.67 \pm 0.22) \times 10^3 N_H$. The central density is obtained from the X-ray

luminosity and has a strong dependence on the distance. Watt et al. (1992) assumed a Hubble constant of h=50 km s^{-1} Mpc^{-1}. With a mean velocity of 6,853 km s^{-1} (Colless & Dunn 1996) and with this Hubble constant, the distance to the Coma cluster is 137 Mpc. Recently Rood (1988) using the Tully–Fisher relation to measure the distance modulus to the galaxies in the Coma cluster, to observe a value of 34.4±0.2 mag whereas Liu & Graham (2001) using infrared surface brightness fluctuations get 34.99±0.21 mag. The average is 34.7 mag that corresponds to a distance of 87.1 Mpc. This is consistent with the distance of 85.6 Mpc given by Freedman et al. (2001).

The galactic velocity data are taken from Beijersbergen (2003) who provide information for 583 galaxies. The velocity centroid of the Coma cluster is $12^h59^m19^s$, $27°52'2''$ (J2000). They find that early-type galaxies (E+S0+E/S0) have a mean velocity of 9,926 km s^{-1} and a rms (root-mean-square) velocity, of 893 km s^{-1}. Let us assume that all the galactic velocities are due to Curvature-redshift. That is we assume that the actual velocities, the peculiar velocities, are negligible. Then the redshifts for the galaxies are calculated (in velocity units) by

$$v = v_0 + \int_0^Z 51.691\sqrt{N(Z)}\,dZ\,\mathrm{km\,s^{-1}}, \qquad (46)$$

where Z is the distance from the central plane of the Coma cluster to the galaxy measured in Mpc, $N(Z)$ is the density of the intergalactic gas cloud and v_0 is the average velocity of the galaxies in the cluster. The problem here is that we do not know Z distances. Nevertheless, we can still get a good estimate by assuming that the distribution in Z is statistically identical to that in X and in Y. In a Monte Carlo simulation, each galaxy was given a Z distance that was the same as the X (or Y) distance of one of the other galaxies in the sample chosen at random. For 50 trials, the computed dispersion was $554 km\,s^{-1}$ which can be compared with the measured dispersion of $893 km\,s^{-1}$. Curvature-cosmology has predicted the observed dispersion of galactic velocities in the Coma cluster to within a factor of two.

Considering that this is a prediction of the cosmological model without fitting any parameters and ignoring all the complications of the structure both in the gas and galactic distributions the agreement is remarkable.

Since the distance to the Coma cluster is an important variable, the computed velocity dispersion from the Monte Carlo simulation for some different distances (all the other parameters are the same) is shown in Table 9. Thus, the redshift dispersion (in velocity units) is approximately a linear function of the Coma distance.

Table 9. Coma velocity dispersions for some distances.

Distance/Mpc	50	87	100	150
Dispersion /km s^{-1}	318	554	636	955

This is not surprising since in this context the distance is mainly a scale factor.

Beijersbergen (2003) note that a better fit to the velocity distribution is provided by the sum of two Gaussian curves. Their best fit parameters for these two Gaussians are $v_1 = 7,501 \pm 187\,\mathrm{km\,s^{-1}}$, with $\sigma_1 = 650 \pm 216\,\mathrm{km\,s^{-1}}$ and $v_2 = 6641 \pm 470\,\mathrm{km\,s^{-1}}$, with $\sigma_2 = 1,004 \pm 120\,\mathrm{km\,s^{-1}}$. This double structure is supported by Colless & Dunn (1996) who argue for an ongoing merger between two sub clusters centered in projection on the dominant galaxies NGC 4874 and NGC 4889.

In addition, Briel, Henry, & Boehringer (1992) found evidence for substructure in the X-ray emission and Finoguenov et al. (2004) and White, Briel, & Henry (1993) have measured the X-ray luminosity of individual galaxies in the Coma cluster showing that the model for the gas used above is too simple. The net effect of this substructure is that the observed velocity dispersion would be different from that predicted by a simple symmetric model. Thus, it appears that substructure makes it very difficult to achieve a more accurate test of Curvature-cosmology using the Coma cluster.

There is an important difference between Curvature-redshift and models that assume that the redshifts of the galaxies within a cluster are due to their velocities. Since the laws of celestial mechanics are symmetric in time, any galaxy could equally likely be going in the opposite direction. Thus a galaxy with a high relative (Z) velocity could be in the near side of the cluster or equally likely on the far side of the cluster. However, if the redshifts are determined by Curvature-redshift then there will be a strong correlation in that the higher redshifts will come from galaxies on the far side of the cluster.

A possible test is to see if the apparent magnitudes are a function of relative redshift. With a distance of 87.1 Mpc the required change in magnitude is about 0.025 mag Mpc^{-1}. A simple regression between magnitude of Coma galaxies (each relative to its type average) and velocity did not show any significant dependence.

Although this was disappointing, several factors can explain the null result. The first is the presence of the substructure; the second is that the magnitudes for a given galactic type have a standard deviation of about one magnitude, which in itself is sufficient to wash out the predicted effect; and thirdly mistyping will produce erroneous magnitudes due to the different average veloc-

ities of different types. In support of the second factor, we note that for 335 galaxies with known types and magnitudes, the standard deviation of the magnitude is 1.08 mag and if we assume that the variance of the Z distribution is equal to the average of the variances for the X and Y distributions then the expected standard deviation of the slope is $0.076 \text{ mag Mpc}^{-1}$. Clearly, this is such larger than the expected result of $0.025 \text{ mag Mpc}^{-1}$. It is expected that better measurements or new techniques of measuring differential distances will in the future make this a very important cosmological test.

In ΛCDM observations of the velocity dispersion of clusters of galaxies cannot be explained without invoking an ad hoc premise such as dark matter. However Curvature-cosmology not only explains the observations but also makes a good prediction, without any free parameters, of its numerical value.

5.6. Angular size

Closely related to surface brightness is relationship between the observed angular size of a distant object and its actual linear transverse size.

The major distinction in angular size is that Curvature-cosmology, like all tired-light cosmologies, does not include the $(1 + z)$ aberration factor. Its relationship between the observed angular size and the linear size is very close (for small redshifts) to the Euclidean equation.

Gurvits, Kellermann, & Frey (1999) provide a comprehensive history of studies for a wide range of objects that generally show a $1/z$ or Euclidean dependence. Most observers suggest that the probable cause is some form of size evolution. Recently López-Corredoira (2010) used 393 galaxies with redshift range of $0.2 < z < 3.2$ in order to test many cosmologies.

Briefly, his conclusions are

: *The average angular size of galaxies is approximately proportional to $z^{-\alpha}$ with α between 0.7 and 1.2.*

: *Any model of an expanding universe without evolution is totally unable to fit the angular size data ...*

: *Static Euclidean models with a linear Hubble law or simple tired-light fit the shape of the angular size vs z dependence very well: there is a difference in amplitude of 20%–30%, which is within the possible systematic errors.*

: *It is also remarkable that the explanation of the test results with an expanding model require four coincidences:*

  1. *The combination of expansion and (very strong evolution) size evolution gives nearly the same result as a static Euclidean universe with a linear Hubble law: $\theta \propto z^{-1}$.*

  2. *This hypothetical evolution in size for galaxies is the same in normal galaxies as in quasars, as in radio galaxies, as in first ranked cluster galaxies, as the separation among bright galaxies in cluster*

  3. *The concordance model gives approximately the same (differences of less than 0.2 mag within $z < 4.5$) distance modulus in a Hubble diagram as the static Euclidean universe with a linear law.*

  4. *The combination of expansion, (very strong) size evolution, and dark matter ratio variation gives the same result for the velocity dispersion in elliptical galaxies (the result is that it is nearly constant with z) as for a simple static model with no evolution in size and no dark matter ratio variation.*

With a redshift range of $z < 3$ the value of S is approximately proportional to $z^{0.68}$ which shows that it is consistent with these results. A full analysis requires a fairly complicated procedure to correct the observed sizes for variations in the absolute luminosity.

A simple example of the angular size test can be done using double-lobed quasars. Using quasar catalogues, Buchalter et al. (1998) carefully selected 103 edge-brightened, double-lobed sources from the VLA FIRST survey and measured their angular sizes directly from the FIRST radio maps.

Since Buchalter et al. (1998) claim that three different Friedmann ΛCDM models fit the data well but that a Euclidean model had a relatively poor fit a reanalysis is warranted.

Their angular sizes were converted to linear sizes for each cosmology and were divided into six bins so that there were 17 quasars in each bin. Because these double-lobed sources are essentially one-dimensional a major part of their variation in size is due to projection effects.

For the moment assume that in each bin they have the same size, $\hat{S}$, and the only variation is due to projection then the observed size is $\hat{S}\sin(\theta)$ where θ is the projection angle. Clearly, we do not know the projection angle but we can assume that all angles are equally likely so that if the N sources, in each bin, are sorted into increasing size the i'th source in this list should have, on average, an angle $\theta_i = \pi(2i-1)/4N$. Thus the maximum likelihood estimate of $\hat{S}$ is

$$\hat{S}_{\text{est}} = \frac{\sum_{i=1}^{N} \sin(\theta_i)S_i}{\sum_{i=1}^{N} \sin^2(\theta_i)}.$$

Note that the sum in the denominator is a constant and that the common procedure of using median values is the same as using only the central term in the sum.

Next a regression was done between logarithm of the estimated linear size in each bin and $\log(1 + z)$ where z is the mean redshift. Then the significance of the test was how close was the exponent, b, to zero. For ΛCDM the exponent was $b = -0.79 \pm 0.44$ and for Curvature-cosmology, it was $b = 0.16 \pm 0.44$. Although the large uncertainties show that this is not a decisive discrimination between the two cosmologies the slope for the Curvature-cosmology suggests that no expansion is more likely.

For angular size the conclusion is in favor of Curvature-cosmology.

5.7. Galaxy distribution

Recently, large telescopes with wide fields and the use of many filters have enabled a new type of galactic survey. The light-collecting capability of the large telescopes enables deep surveys to apparent magnitudes of 24 mag or better and the wide field provides a fast survey over large areas.

A major innovation is the use of many filters whose response can be used to classify the objects with great accuracy. Thus, galaxies can be separated from quasars without needing morphological analysis. This photometric method of analysis works because photometric templates are available for a wide range of types of galaxies and other types of objects. In addition, accurate redshifts are obtained from fitting the templates without the tedious procedure of measuring the spectrum of each object.

A typical example of this photometric method is the COMBO-17 survey (Classifying Objects by Medium-Band Observations in 17 filters) provided by Wolf et al. (2004). The goal of this survey was to provide a sample of 50,000 galaxies and 1000 quasars with rather precise photometric redshifts based on 17 colors.

In practice, such a filter set provides a redshift accuracy of 0.03 for galaxies and 0.1 for quasars. The central wavelength of the 17 filters varied from 364 nm to 914 nm and consisted of 5 broadband filters (U, B, V, R, I) and 12 narrower-band filters. Wolf et al. (2003) have analyzed this data and claim that there is strong evolution for $0.2 < z < 1.2$.

Instead of using generic K-corrections, the intrinsic (rest frame) luminosity of all galaxies are individually measured from their 17-filter spectrum. For each galaxy, three rest-frame pass bands are considered, (i) the SDSS r-band, (ii) the Johnston B-band and (iii) a synthetic

Table 10. M^*_{CC} for SED Type 1 galaxy luminosity distributions.

z	$\Delta\mu$	M_r^{*a}	M_B^*	M_{280}^*
0.3	0.426	-20.49	-19.06	-17.38
0.5	0.642	-20.49	-19.15	-17.84
0.7	0.822	-20.77	-19.37	-17.62
0.9	0.975	-20.54	-19.09	-17.79
1.1	1.107	-20.87	-19.23	-18.23
χ^2		3.70	2.32	12.81

[a]Absolute magnitude for the SDSS r-band

UV continuum band centered at $\lambda_{\mathrm{rest}} = 280$ nm with 40 nm FWHM and rectangular transmission function.

A spectral energy distribution, SED, was determined for each galaxy by template matching. For the evolution analysis, they were assigned to one of four types. The only type that showed a well-defined peak in their luminosity distribution was Type 1 which covers the E-S_a galactic types. The characteristics of the luminosity distribution were obtained by fitting a Schechter function which is

$$\phi(L)dL\phi^*(L/L^*)^\alpha e^{L/L^*}dL$$

where the luminosity L^* (and its magnitude M^*) is a measure of location and α is a measure of shape.

They found that a fixed value for α works quite well for the luminosity functions of individual SED types. Examination of their estimate of M^* for Type 1 galaxies showed that if they were converted to Curvature-cosmology magnitudes they were independent of redshift. This is shown in Table 10 where the data are taken from the appendix to Wolf et al. (2003). The second column is the difference, $\Delta\mu = \mu_{CC} - \mu_{BB}$, between BB and CC, (Curvature-cosmology), distance moduli. The remaining columns show the CC absolute magnitudes for the three rest-frame bands.

The last row shows the χ^2 for the five magnitudes relative to their mean using the given uncertainties (all in the range 0.14-0.23).

With four degrees of freedom, the first two bands show excellent agreement with a constant value. The values for M_{280}^* have less than a 2.5% chance of being constant. However since most of the discrepancy comes from the $z = 0.3$ value of -17.38 mag and most of this band at small redshifts is outside the range of the 17 filters this discrepancy can be ignored.

If this value is ignored, the χ^2 is reduced from 12.81 to 6.12 (with 3 D0F) which is consistent with being constant. Since α is independent of redshift, the result is that if the data had been analyzed using Curvature-cosmology the magnitude for these Type 1 galaxies does not vary with redshift.

Thus we have the surprising result that using ΛCDM a class of galaxies has a well-defined luminosity evolution that can be explained by Curvature-cosmology. In other words, there is no expansion.

5.8. *Quasar variability in time*

One of the major differences between a tired-light cosmology and an expanding universe cosmology is that any expanding universe cosmology predicts that time variations and clocks have the same dependence on redshift as does the frequency of the radiation.

Hawkins (2010, 2003) has analyzed the variability of 800 quasars covering epoch scales from 50 days to 28 years. His data permitted the straightforward use of Fourier analysis to measure the time scale of the variability. He showed that there was no significant change in the time scale of the variability with increasing redshift. He considered and rejected various explanations including that the time scales of variations were shorter in bluer pass bands or that the variations were not intrinsic but were due to intervening processes such as gravitational micro-lensing. His conclusion was either that the quasars are not at cosmological distances or that the expanding universe cosmologies are incorrect in this prediction.

Curvature-cosmology predicts the observed quasar epoch variability of zero.

5.9. *The Butcher-Oemler effect*

If there were evidence of significant change in the universe as a function of redshift, it would be a detrimental to any static cosmology. Probably the most important evidence for this cosmic evolution that appears to be independent of any cosmological model is the Butcher & Oemler (1978) effect. Although the effect has been discussed in earlier papers, the definitive paper is Butcher & Oemler (1984).

They observed that the fraction of blue galaxies in galactic clusters appears to increase with redshift. Clusters allow the study of large numbers of galaxies at a common distance and out to large redshifts, which makes them ideal for studies in evolution. The core regions in a cluster are dominated by early-type (elliptical and lenticular) galaxies, which have a tight correlation between their colors and magnitudes.

We can calculate R_{30}, the projected cluster-centric radius that contains 30% of the total galaxy population. The blue fraction, f_B, is defined to be the fraction of galaxies within R_{30} which are bluer than the color-magnitude relationship for that cluster.

At first sight, this may appear to be a simple test that could be done with apparent magnitudes. However to compare the ratio for distant clusters with that for nearby ones the colors must be measured in the rest frame of each cluster, hence the need to use K-corrections.

The major advantage of the Butcher–Oemler effect is that it is independent of the luminosity-distance relationship that is used. Therefore, to be more precise f_B is the fraction that has an absolute magnitude M_V, whose rest frame (B-V) color is at least 0.2 magnitudes bluer than expected. A review by Pimbblet (2003) summaries the important observations.

In its original form the Butcher–Oemler effect is dependent on the apparent magnitude cut-off limits. It is essential that selection effects are the same in the rest frame for each cluster. There are further complications in that the percentage of blue galaxies may or may not depend on the richness of the cluster and the effect of contamination from background galaxies.

Although Pimbblet (2003) concluded there was a definite effect, his Fig. 1 shows that this conclusion is open to debate. Since then there have been several attempts to measure an unambiguous effect. Even though they attempted to duplicate the original methodology of Butcher & Oemler, Hawkins (2003) found essentially no effect for K-selected galaxies.

Andreon, Lobo, & Iovino (2004) examined three clusters around z=0.7 and did not find clear-cut evidence for the effect. To quote one of their conclusions: *Twenty years after the original intuition by Butcher & Oemler, we are still in the process of ascertaining the reality of the Butcher–Oemler effect.*

The Butcher-Oemler effect remains uncertain, and therefore does not provide evidence to refute a static cosmology.

5.10. *Fluctuations in the CMBR*

In the model proposed for Curvature-cosmology these fluctuations will also occur but in this case they are due to variations in the density of the cosmic plasma. The CMBR seen through the denser gas within a galactic cluster will have lower than average temperature. Cabré et al. (2006) show some support for this model in that they have correlated data from the Wilkinson Microwave Anisotropy Probe (WMAP) with galaxy samples from the SDSS DR4 galaxy survey and found a significant correlation for the intensity fluctuations with galaxy density.

5.11. *Pioneer 10 acceleration.*

Precise tracking of the *Pioneer* 10/11, *Galileo* and *Ulysses* spacecraft (Anderson et al. 2002) have shown an anomalous constant acceleration for *Pioneer* 10 with a magnitude $(8.74 \pm 1.55) \times 10^{-10}$ m s^{-2} directed towards the sun.

The only method for monitoring *Pioneer* 10 is to measure the frequency shift of the signal returned by an active phase-locked transponder. These frequency measurements are then processed using celestial mechanics in order to get the spacecraft trajectory.

The simplicity of this acceleration and its magnitude suggests that *Pioneer* 10 could be a suitable candidate for investigating the effects of Curvature-redshift. There is a major problem in that the direction of the acceleration corresponds to a blue shift whereas Curvature-redshift predicts a redshift.

Nevertheless, we will proceed, guided by the counterintuitive observation that a drag force on a satellite actually causes it to speed up. This is because the decrease in total energy makes the satellite change orbit with a redistribution of kinetic and potential energy.

The crucial point of this analysis is that the only information available that can be used to get the *Pioneer* 10 trajectory is Doppler shift radar. There is no direct measurement of distance.

Thus the trajectory is obtained by applying celestial mechanics and requiring that the velocity matches the observed frequency shift. Since the sun produces the dominant acceleration, we can consider that all the other planetary perturbations and know drag effects have been applied to the observations and the required celestial mechanics is to be simple two-body motion.

If the observed velocity (away from the sun) is increased by an additional apparent velocity due to Curvature-redshift the orbit determination program will compensate by assuming that the spacecraft is closer to the sun than its true distance. It will be shown that this distance discrepancy produces an extra apparent acceleration that is directed towards the sun. The test of this model is whether the densities required by Curvature-redshift agree with the observed densities.

Let the actual velocity of *Pioneer* 10 at a distance r, be denoted by $v(r)$, then since the effect of Curvature-redshift is seen as an additional velocity, $\Delta v(r)$ where from Eq. 10

$$\Delta v(r) = 2\sqrt{8\pi G} \int_0^r \sqrt{\rho(r)} \, dr, \qquad (47)$$

where the factor of 2 allows for the two-way trip and the density at the distance r from the sun is $\rho(r)$. Since *Pioneer* 10 has a velocity away from the sun, this redshift shows an increase in the magnitude of its velocity.

We will assume that all the perturbations and any other accelerations that may influence the *Pioneer* 10 velocity have been removed as corrections to the observed velocity and the remaining velocity, $v(r)$, is due to the gravitational attraction of the sun. In this case

the energy equation is

$$v(r)^2 = v_\infty^2 + \frac{2\mu}{r}, \qquad (48)$$

where $\mu = GM$ is the gravitational constant times the mass of the sun ($\mu = 1.327 \times 10^{20} \, \mathrm{m^3 \, s^{-2}}$) and v_∞ is the velocity at infinity.

The essence of this argument is that the tracking program is written to keep energy conserved so that an anomalous change in velocity, $\Delta v(r)$, will be interpreted as a change in radial distance which is

$$\Delta r = -\sqrt{\frac{2r^3}{\mu}} \, \Delta v(r).$$

Thus an increase in magnitude of the velocity will be treated as a decrease in radial distance which, in order to keep the total energy constant, implies an increase in the magnitude of the acceleration. Either by using Newton's gravitational equation or by differentiating Eq. 48 the acceleration $a(r)$ is given by

$$a(r) = -\frac{\mu}{r^2}. \qquad (49)$$

Hence with $v_\infty = 0$ and therefore $v(r) = \sqrt{2\mu}/r$ we get

$$\Delta a(r) = \frac{2\mu}{r^3} \, \Delta r = \sqrt{\frac{8\mu}{r^3}} \, \Delta r,$$

and then to the first order an increase in velocity of $\Delta v(r)$ will produce an apparent decrease in acceleration of $\Delta a(r)$, and

$$\begin{aligned}
\Delta a &= 8\sqrt{\pi \mu G} \, r^{-3/2} \int_0^r \sqrt{\rho(r)} \, dr \\
&= 16\sqrt{\pi \mu G} \, r^{-1/2} < \sqrt{\rho(r)} > \\
&= 6.90 R^{-1/2} < \sqrt{\rho(r)} >,
\end{aligned}$$

where for the last equations we measure the distance in AU so that $r = 1.496 \times 10^{11} R$ and the angle brackets show an average value.

Now fig. 7 from (Anderson et al. 2002) shows that after about 20 AU the anomalous acceleration is essentially constant. The first step is to get an estimate of the required density and see if is feasible.

Using the observed acceleration of $a_\mathrm{P} = 8.74 \times 10^{-10}$ m s^{-2} the required average density for the two-way path is $1.60 \times 10^{-20} R \, \mathrm{kg \, m^{-3}}$ and for R=20 it is $3.21 \times 10^{-19} \, \mathrm{kg \, m^{-3}}$.

The only constituent of the interplanetary medium that approaches this density is dust. One estimate by Le Sergeant D'Hendecourt & Lamy (1980) of the interplanetary dust density at 1 AU is $1.3 \times 10^{-19} \, \mathrm{kg \, m^{-3}}$

and more recently, Grun et al. (1999) suggests a value of 10^{-19} kg m^{-3} which is consistent with their earlier estimate of 9.6×10^{-20} kg m^{-3} (Grun, Zook, Fechtig, & Giese 1985).

Although the authors do not provide uncertainties, it is clear that their densities could be in error by a factor of two or more. The main difficulties are the paucity of information and that the observations do not span the complete range of grain sizes.

The meteoroid experiment on board *Pioneer* 10 measures the flux of grains with masses larger than 10^{-10} g. The results show that after it left the influence of Jupiter the flux (Anderson et al. 2002) was essentially constant (in fact there may be a slight rise) out to a distance of 18 AU.

It is thought that most of the grains are being continuously produced in the Kuiper belt. As the dust orbits evolve inwards due to Poynting-Robertson drag and planetary perturbations, they achieve a roughly constant spatial density. The conclusion is that interplanetary dust could provide the required density to explain the anomalous acceleration by a frequency shift due to Curvature- redshift.

Overall, this analysis has shown that it is possible to explain the acceleration anomaly of *Pioneer* 10 but that a more definitive result requires Curvature-redshift to be included in the fitting program and more accurate estimates of the dust density are certainly needed. Subject to the caveat about the dust density, Curvature-redshift could explain the anomaly in the acceleration of *Pioneer* 10 (and by inference other spacecraft).

Not only can Curvature-cosmology explain the anomalous Pioneer 10 acceleration, it has a feasible prediction of its value.

5.12. *The Sunyaev–Zel'dovich effect*

The Sunyaev–Zel'dovich effect (Sunyaev & Zeldovich 1970; Peebles 1993) is the effect of Thompson scattering of background radiation by free electrons in the intervening medium. The technique depends on knowing the spectrum of the background source and then measuring the changes in the spectrum due to the intervening plasma.

In particular, it is the scattering in both angle and frequency of the cosmic microwave background radiation (CMBR) by electrons in the cosmic plasma. Because of the rapidly changing density (like $(1+z)^3$) with redshift this is an important effect in ΛCDM cosmology. The effect is often characterized by the dimensionless Compton y-parameter, which for a distance x through non-relativistic thermal plasma with an electron density

of N_H has the value

$$y = \frac{kT_e}{m_e c^2}\sigma_T N_H x = 3.46 \times 10^{-16} N_H T_e x \, \mathrm{Mpc}, \quad (50)$$

where σ_T is the Thompson cross-section. An object at redshift z is at the distance $x = R\chi = 5.80 \times 10^3 N_H^{1/2} \log(1+z)$ Mpc. Hence, using $T_e = 2.62 \times 10^9$ K, $N_H = 1.35 \, \mathrm{m}^{-3}$ we get $y = 9.2 \times 10^{-6} \log(1+z)$.

Using the CMBR as a source the Sunyaev–Zel'dovich effect has been observed and Mather et al. (1990) report an observed upper limit of $y = 0.001$, and more recently Fixsen et al. (1996) report $y = 1.5 \times 10^{-5}$.

Using this limit with Eq. 50 shows that there is no effect in Curvature-cosmology if $z < 4.1$. Although in Curvature-cosmology the CMBR has a more local origin it is of interest to note that this analysis assumes that each photon has many Compton interactions. but

(Longair 1991; Sunyaev & Zeldovich 1980). Bielby & Shanks (2007) extend the results of Lieu, Mittaz, & Zhang (2006) to show that not only was the Sunyaev–Zel'dovich effect less than what was expected but that it tendered to disappear as the redshift went from 0.1 to 0.3. The conclusion is that Curvature-cosmology is completely consistent with the experimental observations of the Sunyaev–Zel'dovich effect on the CMBR. Thus the Sunyaev–Zel'dovich effect may be important in standard cosmology but it is not important in Curvature-cosmology.

5.13. *Gravitational lensing.*

There are many gravitational lens where a quasar or distant galaxy has one or more images produced by a nearer lensing galaxy or cluster of galaxies. A set of these lensing systems has been examined in the context of Curvature-cosmology to see if it offers a consistent and possibly simpler explanation. The two important measures are the prediction of the mass of the lensing galaxy and the determination of the Hubble constant from the time delays between variations in the luminosity of different images. Since the delay measurement is easily done, all that is needed is to measure the different path lengths. This path difference involves both geometric and general relativistic corrections.

One of the remarkable properties of gravitational lenses is that the geometry is completely determined by a two-dimensional lensing potential which can be expressed in terms of a surface density at the position of the lensing galaxy. For thin lenses, any two systems with the same surface density distribution have the same lens effect. Now the usual way to determine the surface density is to measure the widths of spectral lines, assume that the width is due to velocity and then use the virial theorem to obtain the surface density.

28

However in Curvature-cosmology the widths of spectral lines are likely to have a large component due to the effects of Curvature-redshift from dust and gas in the lensing object. Thus the widths are not a reliable measure of area density and this method cannot be used.

5.14. *Lyman_alpha forest*

. The Lyman-α (Lyα) forest is the large number of absorption lines seen in the spectra of quasars. Most of the lines are due to absorption by clouds of neutral hydrogen in the line of sight to the quasar. Some of the lines are due to other elements or due to Lyman-β absorption.

Because of the redshift between the absorbing cloud and us, the lines are spread out over a range of wavelengths. Usually the analysis is confined to lines between the Lyα (at a wavelength of 121.6 nm) and Lyβ (at 102.5 nm). Thus, each quasar provides a relatively narrow spectrum of Ly-α lines at a redshift just less than that for the quasar. Since the advent of spacecraft telescopes, in which can observe the ultraviolet lines, and by using many quasars the complete redshift range up to the most distant quasar has been covered. The large redshift range makes the Lyman α spectra potentially a powerful cosmological tool.

The obvious cosmological observation is the density of lines as a function of redshift but as discussed by Rauch (1998) in an excellent review, there are many important observational problems.

The first, which has now been overcome, is that the spectra must have sufficient resolution to resolve every line. The second is that most lines are very weak and the number of resolved lines can depend greatly on the signal-to-noise ratio. This is accentuated because the steep spectrum for the density of lines as a function of their strength means that a small decrease in the acceptance level can drastically increase the number of observed lines. The third problem is that each quasar only provides a set of lines in a narrow range of redshift and there are considerable difficulties in getting uniform cross-calibrations.

In addition to these problems, it will be shown that Curvature-redshift can have a profound effect on the interpretation of the line widths and column densities.

Since in Curvature-cosmology, the distribution of clouds is independent of time or distance the expected density of lines as a function of redshift is

$$\frac{dn}{dz} = \frac{AcN_H}{H(1+z)}, \qquad (51)$$

where N_c is the volume density and A is the average area of a cloud. Most observers have fitted a power law

with the form $(1+z)^\gamma$ to the observed line densities with a wide range of results. They vary from $\gamma = 1.89$ to $\gamma = 5.5$ (Rauch 1998). All of which are inconsistent with the Curvature-cosmology prediction of $\gamma = -1$.

In Curvature-cosmology, there is the additional effect that much of the line broadening may be due to Curvature-redshift. Curvature-redshift will be operating within the clouds so that the observed line width will be a combination of the usual Voigt profile and the change in the effective central frequency as the photons pass through the cloud. If the cloud has a density $\rho(x)$ at the point x, measured along the photon trajectory then the change in frequency from the entering frequency due to Curvature-redshift is

$$\frac{\Delta\nu}{\nu} = \frac{1}{c}\int \sqrt{8\pi G\rho(x)}dx.$$

In units of $N(x) = \rho(x)/m_H$ this is (with N in m^{-3} and dx in kpc)

$$\frac{\Delta\nu}{\nu} = -\frac{\Delta\lambda}{\lambda} = \int 1.724 \times 10^{-7}\sqrt{N(x)}dx.$$

Then the final profile will be the combination of the natural line width, the Doppler width due to temperature, any width due to bulk motions and the Curvature-redshift width. Now assuming pure hydrogen, the hydrogen column density is given by $N_H = \int N(x)dx$.

Although it is unlikely that the line of sight goes through the center of the cloud, it is reasonable to expect a roughly symmetric distribution of gas with a shape similar to a Gaussian. We can define an effective density width by

$$x_w^2 = \int (x-\overline{x})^2 N(x)dx \bigg/ \int N(x)dx.$$

Also define $N_c = N_H/x_w$ and an effective velocity width $\Delta v = 51.68\eta x_w\sqrt{N_c}$ and where η is a small numeric constant that depends on the exact shape of the density distribution. Eliminating the central density, we get (with x_w in kpc)

$$\Delta v^2 = 8.656 \times 10^{-17}\eta^2 N_H x_w. \qquad (52)$$

For values $N_H = 10^{19}$ m^{-2}, x_w=1 kpc and with η=1 we get Δv=29 km s^{-1}.

Since there is a wide variation in column densities and the effective widths are poorly known, it is clear that Curvature-redshift could completely dominate many of the Lyman-α line widths and the others would require a convolution of the Doppler profile with the Curvature-redshift density effect. What is also apparent is that the very broad absorption lines may be due to Curvature-redshift acting in very dense clouds.

Although there is uncertainty about the observed relationship between the line width and the column density, we note that for a fixed effective density width, Eq. 52 predicts a square relationship that may be compared with the exponent of 2.1 ± 0.3 found by Pettini et al. (1990). Clearly, there needs to be a complete re-evaluation of profile shapes, column densities, and cloud statistics that allows for the effects of Curvature-cosmology. We must await this analysis to see whether the Lyman-α forest can provide a critical test of Curvature-cosmology.

5.15. *Nuclear abundances*

One of the successes of ΛCDM cosmology is in its explanation of the primordial abundances of the light elements. Since the proposed Curvature-cosmology is static, there must be another method of getting the 'primordial' abundances of light elements. In Curvature-cosmology, the primordial abundance refers to the abundance in the cosmic gas from which the galaxies are formed.

The first point to note is that in Curvature-cosmology the predicted temperature of the cosmic plasma is 2.465×10^9K at which temperature nuclear reactions can proceed.

It is postulated that in Curvature-cosmology there is a continuous recycling of material from the cosmic plasma to galaxies and stars and then back to the plasma. Because of the high temperature, nuclear reactions will take place whereby the more complex nuclei are broken down to hydrogen.

5.16. *Galactic rotation curves*

One of the most puzzling questions in astronomy is: why does the observed velocity of rotation in spiral galaxies not go to zero towards the edge of the galaxy. Simple Keplerian mechanics suggest that there should be a rapid rise to a maximum and then a decrease in velocity that is inversely proportional to the square root of the radius once nearly all the mass has been passed.

Although the details vary between galaxies, the observations typically show a rapid rise and then an essentially constant tangential velocity as a function of radius out to distances where the velocity cannot be measured due to lack of material. The ΛCDM explanation is that this is due to the gravitational attraction of a halo of dark matter that extends well beyond the galaxy. We examine whether this rotation curve can be explained by Curvature-redshift.

Observations show that our own Galaxy and other spiral galaxies have a gas halo that is larger than the main concentration of stars. It is clear that if the observed

redshifts are due to Curvature-redshift acting within this halo, the halo must be asymmetric; otherwise, it could not produce the asymmetric rotation curve.

Now the observed velocities in the flat part of the curves are typically 100 to 200 km s^{-1}. The first step is to see if Curvature-redshift provides the right magnitude for the velocity. For a gas with an average density of N_H the predicted redshift (in velocity units) is $5.17 \times 10^{-2} d\sqrt{N} \, \text{km s}^{-1}$ where d is the distance in kpc. For realistic values of $d = 10$ kpc and $N = 1.0 \times 10^5$ m^{-3} the velocity is 163 km s^{-1}. Thus, the magnitude is feasible.

Although there could be a natural asymmetry in a particular galaxy, the fact that the flattened rotation curve is seen for most spiral galaxies suggests that there is a common cause for the asymmetry.

A partial explanation is that the halos are rotating more like a solid object and that the observed rotation is genuine.

Another possibility is that the asymmetry could arise from ram pressure. Since most galaxies are moving relative to the cosmic medium, it is expected that there will be an enhanced density towards the leading point of the galaxy. This asymmetric density could produce an apparent velocity gradient across the galaxy that could explain the apparent rotation curve.

Naturally, there would be range of orientations and the apparent velocity gradient must be added to any intrinsic rotation curve to produce a wide diversity of results. Thus, Curvature-redshift could explain the galactic rotation curves if there is an asymmetric distribution of material in the galactic halo.

Both cosmologies have problems with galactic rotation curves. ΛCDM cosmology not only requires dark matter but does not have any definite models for its distribution. Curvature-cosmology has the problem of achieving sufficient asymmetry to mimic a rotation curve.

5.17. *Redshifts in our Galaxy*

In our Galaxy, the Milky Way, there is an interesting prediction. The density of the interstellar ionized gas is high enough to inhibit Curvature-redshift for radio frequencies.

From Eq. 31 it was shown that for wavelengths longer than about $20.6 N_H^{-1/2}$ m the effect of refractive index in fully ionized plasma will inhibit Curvature-redshift. The refractive index of neutral hydrogen is too low to inhibit Curvature-redshift. However, any fully ionized plasma with $N_H > 10^4 \text{m}^{-3}$ will inhibit Curvature-redshift for the 21 cm hydrogen line. Since the local interstellar medium has an electron density of about 10^5 m^{-3}

Curvature-redshift will be inhibited for the 21 cm hydrogen in these local regions.

Thus for sight lines close to the Galactic plane we can assume a similar density and thus a similar inhibition with the result that the observed radio redshifts can be correctly interpreted as genuine velocities. Thus, there is little change needed to the current picture of galactic structure and rotation derived from 21 cm redshifts. However, there may be some Curvature-redshift present in sight lines away from the plane and especially in the Galactic halo.

Since optical redshifts have the full effects of Curvature-redshift, it should be possible to find objects with discrepant redshifts where the optical redshift is greater than the radio redshift. The difficulty is that the two types of radiation are produced in radically different environments: the optical in compact high temperature objects, such as stars, and the radio in very low-density cold clouds. In addition, there is the complication that within the galactic plane, optical extinction due to dust limits the optical range to about 1 kpc.

Curvature-redshift may help to explain an old stellar mystery. There is a long history provided by Arp (1992) of observations of anomalous redshifts in bright hot stars, which is called the K-term or K-effect.

Allen (1976) states that B_0 stars typically show an excess redshift of 5.1 $\mathrm{m\,s^{-1}}$, A_0 have 1.4 $\mathrm{km\,s^{-1}}$ and F_0 have 0.3 $\mathrm{km\,s^{-1}}$. This can be explained if these stars have a large corona that produces a Curvature-redshift.

It is probably no coincidence that such stars have large stellar winds and mass outflows. In order to see if it is feasible let us consider a simple model for the outflow in which the material has a constant velocity v_0, and conservation of matter (Gauss's Law) then requires that the density has inverse square law dependence. Although this is incorrect at small stellar radii, it is a reasonable approximation further from the star.

Then if ρ_1 is the density at some inner radius r_1, then integration of Eq. 24 out to a radius r_2, the expected redshift in velocity units is

$$v = \sqrt{\frac{2G\dot{M}}{v_o}} \log\left(\frac{r_2}{r_1}\right),$$

where $\dot{M}$ is the observed stellar mass-loss-rate. Then with $\dot{M}$ in solar masses per year, with v and v_0 in $\mathrm{km\,s^{-1}}$, the redshift is

$$v = 91.7\sqrt{\frac{\dot{M}}{v_o}} \log\left(\frac{r_2}{r_1}\right) \ \mathrm{km\,s^{-1}},$$

With $\dot{M} = 10^{-5} M_\odot\,\mathrm{yr}^{-1}$ Cassinelli (1979), $v_0 = 1\,\mathrm{km\,s^{-1}}$ and $r2/r1 = 10^3$ the predicted redshift (in ve-

Table 11. Velocity at, and average velocity within various projected radii in the Coma cluster (distance = 87.1 Mpc).

Radius[a] /Mpc	Velocity /$\mathrm{km\,s^{-1}}$	Mean velocity /$\mathrm{km\,s^{-1}}$
0.0	2327.7	2327.7
0.5	1477.7	1764.8
1.0	1033.4	1342.5
1.5	803.3	1096.9
2.0	658.6	933.2
2.5	557.0	814.4
3.0	481.0	723.3
3.5	421.7	650.7
4.0	374.0	541.2
4.5	334.8	541.2
5.0	302.0	498.7

[a] projected radius

locity units) is $2\,\mathrm{km\,s^{-1}}$ which is in reasonable agreement with the observed K-effects mentioned above.

5.18. *Voids*

If Curvature-cosmology is valid then the redshift of the galaxies in the Coma cluster (Section 5.5) will have been increased, on average, by the additional redshift due to the intergalactic gas. Thus, they will have, on average, a larger redshift than an isolated galaxy at the same distance.

Table 11 shows the predicted (effective) velocity for a galaxy in the center plane of the Coma cluster as a function of the projected radius. The second column is the velocity at that exact radius and the third column shows the average velocity of galaxies (uniformly spread in area) within that radius. This simulation also showed that the average velocity offset for the galaxies in the Coma cluster is 1206 $\mathrm{kms^{-1}}$ which means that the redshift of the center of the Coma cluster is 6926-1206=5720 $\mathrm{kms^{-1}}$. This offset is important for calculating the Hubble constant which from these figures is $5270/87.1=65.7\ \mathrm{kms^{-1}\,Mpc^{-1}}$.

In addition, the redshift of objects seen through a cluster will be increased by Curvature-redshift from the intergalactic gas.

Karoji, Nottale, & Vigier (1976) claim to have seen this effect. They examined radio galaxies and classified them into region A if their light does not pass through a cluster and region B if their light passes through a cluster. They found no significant differences in magnitudes between the two regions but they did find a significant difference in the average redshift that was consistent over the complete range.

Their result is that radio galaxies seen through a cluster had an average extra redshift (in velocity units) of 2412 ± 1327 km s^{-1}. Overall the difference in the distance modulus was $\mu = 0.16 \pm 0.04$, which is just significant.

Since the density and distribution of the gas in the clusters is unknown and the limiting radius of the cluster is not stated, it is impossible to get an accurate prediction.

Nevertheless, we note that for the Coma cluster with a radius of 2 Mpc the average extra redshift (from Table 11 with a factor of two) corresponds to 1866 km s^{-1} showing that Curvature-cosmology could explain the effect.

In a different study, Nottale (1976) and Nottale & Vigier (1977) compared the magnitude of the brightest galaxy in a cluster with that in another cluster with similar redshift. They found that there was no significant difference in magnitudes between clusters but that the clusters with the largest number of galaxies had the higher redshift difference between the pairs.

On average the redshift difference (in velocity units) was 292 ± 85 km s^{-1}. This can be explained by the expected correlation between the number of galaxies and size and density of the intergalactic gas. However it should be noted that these observations have been disputed by Rood & Struble (1982).

In his review of voids in the distribution of galaxies, Rood (1988) quotes Mayall (1960) who observed a large void in the distribution of galaxies in front of the Coma cluster. This void has a magnitude of about 3000 kms^{-1}, which although somewhat larger, is not inconsistent with the expected value of about 1200 km s^{-1}.

In other words, the Coma cluster galaxies have an extra Curvature-redshift due to the intergalactic gas. However, the galaxies just outside the cluster nearer to us do not have this extra redshift and would appear to be closer to us. Hence, we see an apparent void in the redshift distribution in front of the Coma cluster.

A consequence of gas clouds and Curvature-redshift is that the distribution of redshifts is similar to but not identical to the distribution of z distances. Galaxies that are behind a cloud will have a higher redshift than would be expected from a simple redshift distance relationship.

Thus, we would expect to see anomalous voids and enhancements in the redshift distribution. This will be accentuated if the gas clouds have a higher than average density of galaxies.

de Lapparent et al. (1986) show a redshift plot for a region of the sky that includes the Coma cluster. Their data are from the Center for Astrophysics redshift survey and their plot clearly shows several voids. They suggest that the galaxies are distributed on the surfaces of shells. However, this distribution could also arise from the effects of Curvature-redshift in clouds of gas.

5.19. *Entropy*

Consider a stellar cluster or an isolated cloud of gas in which collisions are negligible or elastic. In either case the virial theorem states that the average kinetic energy K, is related to the average potential energy V, by the equation $V = V_0 - 2K$ where V_0 is the potential energy when there is zero kinetic energy. Let U be the total energy then $U = K + V = V_0 - K$. Thus, we get the somewhat paradoxical situation that since V_0 is constant; an increase in total energy can cause a decrease in kinetic energy. This happens because the average potential energy has increased by approximately twice as much as the loss in kinetic energy. Since the temperature is proportional to (or at the least a monotonic increasing function of) the average kinetic energy, it is apparent that an increase in total energy leads to a decrease in temperature. This explains the often-quoted remark that a self-gravitationally bound gas cloud has a negative specific heat capacity. Thus, when gravity is involved the whole construct of thermodynamics and entropy needs to be reconsidered.

One of the common statements of the second law of thermodynamics is that (Longair 1991): *The energy of the universe is Constant: the entropy of the Universe tends to a maximum*, (Feynman 1965): *the entropy of the universe is always increasing* or from Wikipedia *the second law of thermodynamics is an expression of the universal law of increasing entropy, stating that the entropy of an isolated system which is not in equilibrium will tend to increase over time, approaching a maximum value at equilibrium.*

Now the normal proof of the second law considers the operation of reversible and non-reversible heat engines working between two or more heat reservoirs. If we use a self-gravitating gas cloud as a heat reservoir then we will get quite different results since the extraction of energy from it will lead to an increase in its temperature. Thus if the universe is dominated by gravity the second law of thermodynamics needs reconsideration. In addition, it should be noted that we cannot have a shield that hides gravity. To put it another way there is no adiabatic container that is beyond the influence of external gravitational fields. Thus we cannot have an isolated system.

This discussion shows that in a static finite universe dominated by gravity simple discussions of the second law of thermodynamics can be misleading. The presence of gravity means that it is impossible to have an isolated

system. To be convincing any proof of the second law of thermodynamics should include the universe and its gravitational interactions in the proof.

5.20. *Olber's Paradox*

For Curvature-cosmology, Olber's Paradox is not a problem. Curvature-redshift is sufficient to move distant starlight out of the visible band. Visible light from distant galaxies is shifted into the infrared where it is no longer seen. Of course, with a finite universe, there is the problem of conservation of energy and why we are not saturated with very low frequency radiation produced by Curvature-redshift. These low-energy photons are eventually absorbed by the cosmic plasma. Everything is recycled. The plasma radiates energy into the microwave background radiation and into X-rays. The galaxies develop from the cosmic plasma and pass through their normal evolution. Eventually all their material is returned to the cosmic plasma. Curvature-pressure causes most of the material from highly compact objects to be returned to the surrounding region as jets.

5.21. *Philip's relation*

Phillips (1993) Showed that there was a good correlation between the peak magnitude and the width of the light curve for Type Ia supernova. For the Philip's relation to be meaningful, it must be between the absolute magnitude and the width corrected for its $(1 + z)$ dependence.

The slope of the regression of the absolute magnitudes (using the oCDM model and the intrinsic analysis) of Type Ia supernova for all the supernova versus the widths divided by $(1+z)$ is (-0.009 ± 0.091). Which shows that for these observations of Type I a supernova there is no significant Phillip's relation which implies that SALT2 estimates of this relation may be an artifact of the SALT2 analysis.

6. AUTHOR BIOGRAPHY

David F. Crawford was born at Griffth, NSW, Australia in 1937. He graduated BSc and PhD from School of Physics, University of Sydney. Half of his PhD thesis was on designing and building a Geiger counter array to study cosmic ray air-showers and the second half on programming a three-dimensional Monte Carlo simulation on the computer Silliac to calculate the energy and structure of electron-photon cascades. The results published in a 1,512-page book "Electron-photon Shower Distribution Function" by H. Messel and D.F. Crawford, Pergamon Press, 1970.

He worked for two years from 1966 at Cornell University learning radar Astronomy. From 1969 to his retirement in 2003, He provided computer analysis of observations from the Molonglo Radio Telescope. He is a member of the Australian Astronomical Society. He has been an author in 33 papers published in refereed journals. Since he wrote his first program in 1959, He has had a major interest in computers and programming especially in the use of computers to analyze observations and apply them to astrophysical theories. He also have a long-time interest in the foundations of cosmology.

REFERENCES

Allen, C. W. 1976, Astrophysical Quantities

Amanullah, R., Lidman, C., Rubin, D., et al. 2010, The Astrophysical Journal, 716, 712, doi: 10.1088/0004-637X/716/1/712

Anderson, J. D., Laing, P. A., Lau, E. L., et al. 2002, PhRvD, 65, 082004, doi: 10.1103/PhysRevD.65.082004

Andreon, S., Lobo, C., & Iovino, A. 2004, MNRAS, 349, 889, doi: 10.1111/j.1365-2966.2004.07554.x

Arp, H. 1987, Quasars, redshifts, and controversies

—. 1992, Monthly Notices of the Royal Astronomical Society, 258, 800, doi: 10.1093/mnras/258.4.800

Beijersbergen, M. 2003, PhD thesis, University of Groningen, Netherlands

Betoule, M., Kessler, R., Guy, J., et al. 2014, Astromomy and Astrophysics, 568, A22, doi: 10.1051/0004-6361/201423413

Bielby, R. M., & Shanks, T. 2007, Monthly Notices of the Royal Astronomical Society, 382, 1196, doi: 10.1111/j.1365-2966.2007.12456.x

Blanton, M. R., & Moustakas, J. 2009, Annual Review of Astronomy and Astrophysics, 47, 159, doi: 10.1146/annurev-astro-082708-101734

Blondin, S., Davis, T. M., Krisciunas, K., et al. 2008, The Astrophysical Journal, 682, 724, doi: 10.1086/589568

Born, M., & Wolf, E. 1999, Principles of Optics

Braginskij, V. B., & Panov, V. I. 1971, Uspekhi Fizicheskikh Nauk, 105, 779

Briel, U. G., Henry, J. P., & Boehringer, H. 1992, A&A, 259, L31

Buchalter, A., Helfand, D. J., Becker, R. H., & White, R. L. 1998, The Astrophysical Journal, 494, 503, doi: 10.1086/305236

Butcher, H., & Oemler, A., J. 1978, The Astrophysical Journal, 219, 18, doi: 10.1086/155751

—. 1984, The Astrophysical Journal, 285, 426, doi: 10.1086/162519

Cabré, A., Gaztañaga, E., Manera, M., Fosalba, P., & Castander, F. 2006, Monthly Notices of the Royal Astronomical Society, 372, L23, doi: 10.1111/j.1745-3933.2006.00218.x

Carlip, S. 1998, American Journal of Physics, 66, 409, doi: 10.1119/1.18885

Cassinelli, J. P. 1979, Annual Review of Astronomy and Astrophysics, 17, 275, doi: 10.1146/annurev.aa.17.090179.001423

Chu, Y., Wei, J., Hu, J., Zhu, X., & Arp, H. 1998, The Astrophysical Journal, 500, 596, doi: 10.1086/305779

Colless, M., & Dunn, A. M. 1996, ApJ, 458, 435, doi: 10.1086/176827

Conley, A., Guy, J., Sullivan, M., et al. 2011, The Astrophyics Journal Supplement Series, 192, 1, doi: 10.1088/0067-0049/192/1/1

Cowsik, R., & Kobetich, E. J. 1972, The Astrophysical Journal, 177, 585, doi: 10.1086/151735

Crawford, D. F. 1987a, Australian Journal of Physics, 40, 459, doi: 10.1071/PH870459

—. 1987b, Australian Journal of Physics, 40, 449, doi: 10.1071/PH870449

—. 1991, ApJ, 377, 1, doi: 10.1086/170330

—. 1993, ApJ, 410, 488, doi: 10.1086/172765

—. 1995a, ApJ, 440, 466, doi: 10.1086/175288

—. 1995b, ApJ, 441, 488, doi: 10.1086/175375

—. 1998, arXiv e-prints, astro. https://arxiv.org/abs/astro-ph/9803009

—. 1999a, Australian Journal of Physics, 52, 753, doi: 10.1071/PH98065

—. 1999b, arXiv e-prints, astro. https://arxiv.org/abs/astro-ph/9904150

—. 2006, Curvature Cosmology

—. 2009a, arXiv e-prints, arXiv:0901.4169. https://arxiv.org/abs/0901.4169

—. 2009b, arXiv e-prints, arXiv:0901.4172. https://arxiv.org/abs/0901.4172

de Lapparent, V., Geller, M. J., & Huchra, J. P. 1986, ApJL, 302, L1, doi: 10.1086/184625

Dennis, B. R., Suri, A. N., & Frost, K. J. 1973, The Astrophysical Journal, 186, 97, doi: 10.1086/152480

Dicke, R. H. 1964, Nature, 202, 432, doi: 10.1038/202432a0

Disney, M. J. 2000, General Relativity and Gravitation, 32, 1125, doi: 10.1023/A:1001981929727

Djorgovski, S., & Spinrad, H. 1981, The Astrophysical Journal, 251, 417, doi: 10.1086/159478

Ellis, G. F. R. 1984, Annual Review of Astronomy and Astrophysics, 22, 157, doi: 10.1146/annurev.aa.22.090184.001105

Eötvös, R. V., Pekár, D., & Fekete, E. 1922, Annalen der Physik, 373, 11, doi: 10.1002/andp.19223730903

Feynman, R. P. 1965, Feynman lectures on physics. Volume 3: Quantum mechancis

Field, G. B., & Henry, R. C. 1964, The Astrophysical Journal, 140, 1002, doi: 10.1086/148000

Finoguenov, A., Briel, U. G., Henry, J. P., et al. 2004, Astromomy and Astrophysics, 419, 47, doi: 10.1051/0004-6361:20035765

Fixsen, D. J. 2009, ApJ, 707, 916, doi: 10.1088/0004-637X/707/2/916

Fixsen, D. J., Cheng, E. S., Gales, J. M., et al. 1996, The Astrophysical Journal, 473, 576, doi: 10.1086/178173

Freedman, W. L., Madore, B. F., Gibson, B. K., et al. 2001, The Astrophysical Journal, 553, 47, doi: 10.1086/320638

Fukada, Y., Hayakawa, S., Ikeda, M., et al. 1975, Astrophysics and Space Science, 32, L1, doi: 10.1007/BF00646232

Giacconi, R., Gursky, H., Paolini, F. R., & Rossi, B. B. 1962, Physics Review Letters, 9, 439, doi: 10.1103/PhysRevLett.9.439

Goldhaber, G., Boyle, B., Bunclark, P., et al. 1996, Nuclear Physics B Proceedings Supplements, Vol. 51, 51, 123, doi: 10.1016/S0920-5632(96)00493-8

Goldhaber, G., Groom, D. E., Kim, A., et al. 2001, The Astrophysical Journal, 558, 359, doi: 10.1086/322460

Gould, R. J., & Burbidge, G. R. 1963, The Astrophysical Journal, 138, 969, doi: 10.1086/147698

Gruber, D. E., Matteson, J. L., Peterson, L. E., & Jung, G. V. 1999, The Astrophysical Journal, 520, 124, doi: 10.1086/307450

Grun, E., Kruger, H., Srama, R., et al. 1999, in AAS/Division for Planetary Sciences Meeting Abstracts #31, AAS/Division for Planetary Sciences Meeting Abstracts, 55.03

Grun, E., Zook, H. A., Fechtig, H., & Giese, R. H. 1985, Icarus, 62, 244, doi: 10.1016/0019-1035(85)90121-6

Gurvits, L. I., Kellermann, K. I., & Frey, S. 1999, Astromomy and Astrophysics, 342, 378. https://arxiv.org/abs/astro-ph/9812018

Guy, J., Astier, P., Baumont, S., et al. 2007, Astromomy and Astrophysics, 466, 11, doi: 10.1051/0004-6361:20066930

Guy, J., Sullivan, M., Conley, A., et al. 2010, Astromomy and Astrophysics, 523, A7, doi: 10.1051/0004-6361/201014468

Havas, P. 1966, American Journal of Physics, 34, 753, doi: 10.1119/1.1973468

Hawkins, M. R. S. 2003, MNRAS, 344, 492, doi: 10.1046/j.1365-8711.2003.06828.x

—. 2010, MNRAS, 405, 1940, doi: 10.1111/j.1365-2966.2010.16581.x

Holt, S. S. 1992, Annals of the New York Academy of Sciences, 655, 263, doi: 10.1111/j.1749-6632.1992.tb17076.x

Hoyle, F. 1962, Astronomy.

Hoyle, F., Burbidge, G., Narlikar, J. V., & Livio, M. 2000, Physics Today, 53, 71, doi: 10.1063/1.1341928

Hughes, J. P. 1989, The Astrophysical Journal, 337, 21, doi: 10.1086/167084

Itoh, N., Sakamoto, T., Kusano, S., Nozawa, S., & Kohyama, Y. 2000, The Astrophysical Journal Supplement Series, 128, 125, doi: 10.1086/313375

Jackson, J. D. 1975, Classical electrodynamics

Jones, D., Scolnic, D., Riess, A., et al. 2018, in American Astronomical Society Meeting Abstracts #231, Vol. 231, 308.06

Jones, D. O., Rodney, S. A., Riess, A. G., et al. 2013, The Astrophysical Journal, 768, 166, doi: 10.1088/0004-637X/768/2/166

Joseph, R. 2010, Journal of Cosmology, 6, 1547

Kaiser, N., Burgett, W., Chambers, K., et al. 2010, in Ground-based and Airborne Telescopes III, Vol. 7733, 77330E, doi: 10.1117/12.859188

Karoji, H., Nottale, L., & Vigier, J. P. 1976, Astrophysics and Space Science, 44, 229, doi: 10.1007/BF00650484

Kessler, R., Becker, A. C., Cinabro, D., et al. 2009a, The Astrophysical Journal Supplement Series, 185, 32, doi: 10.1088/0067-0049/185/1/32

Kessler, R., Bernstein, J. P., Cinabro, D., et al. 2009b, Publications of the Astronomical Society of the Pacific, 121, 1028, doi: 10.1086/605984

Kinzer, R. L., Jung, G. V., Gruber, D. E., et al. 1997, The Astrophysical Journal, 475, 361, doi: 10.1086/303507

Kormendy, J. 1977, The Astrophysical Journal, 218, 333, doi: 10.1086/155687

Kowalski, M., Rubin, D., Aldering, G., et al. 2008, The Astrophysical Journal, 686, 749, doi: 10.1086/589937

Kuhn, T. S. 1970, The structure of scientific revolutions

Lal, A. K. 2010, Journal of Cosmology, 6, 1533

Le Sergeant D'Hendecourt, L. B., & Lamy, P. L. 1980, Icarus, 43, 350, doi: 10.1016/0019-1035(80)90180-3

Lerner, E. J. 1991, The big bang never happened

Lieu, R., Mittaz, J. P. D., & Zhang, S.-N. 2006, The Astrophysical Journal, 648, 176, doi: 10.1086/505627

Liu, M. C., & Graham, J. R. 2001, The Astrophysical Journal, 557, L31, doi: 10.1086/323174

Longair, M. S. 1991, Astronomy, 19, 95

López-Corredoira, M. 2010, International Journal of Modern Physics D, 19, 245, doi: 10.1142/S0218271810016397

Lubin, L. M., & Sandage, A. 2001a, The Astronomical Journal, 121, 2289, doi: 10.1086/320401

—. 2001b, The Astronomical Journal, 122, 1071, doi: 10.1086/322133

—. 2001c, The Astronomical Journal, 122, 1084, doi: 10.1086/322134

Lyke, B. W., Higley, A. N., McLane, J. N., et al. 2020, The Astrophysical Journal Supplement Series, 250, 8, doi: 10.3847/1538-4365/aba623

Mandrou, P., Vedrenne, G., & Niel, M. 1979, The Astrophysical Journal, 230, 97, doi: 10.1086/157065

Marshall, F. E., Boldt, E. A., Holt, S. S., et al. 1980, The Astrophysical Journal, 235, 4, doi: 10.1086/157601

Mather, J. C., Cheng, E. S., Eplee, R. E., J., et al. 1990, The Astrophysical Journal, 354, L37, doi: 10.1086/185717

Mayall, N. U. 1960, Annales d'Astrophysique, 23, 344

Mazets, E. P., Golenetskii, S. V., Ilinskii, V. N., Gurian, I. A., & Kharitonova, T. V. 1975, Astrophysics and Space Science, 33, 347, doi: 10.1007/BF00640104

Misner, C. W., Thorne, K. S., & Wheeler, J. A. 1973, Gravitation

Nottale, L. 1976, The Astrophysical Journal, 208, L103, doi: 10.1086/182242

Nottale, L., & Vigier, J. P. 1977, Nature, 268, 608, doi: 10.1038/268608a0

Nozawa, S., Itoh, N., & Kohyama, Y. 1998, The Astrophysical Journal, 507, 530, doi: 10.1086/306352

Peebles, P. J. E. 1993, Principles of Physical Cosmology

Petrosian, V. 1976, The Astrophysical Journal, 210, L53, doi: 10.1086/182301

Pettini, M., Hunstead, R. W., Smith, L. J., & Mar, D. P. 1990, Monthly Notices of the Royal Astronomical Society, 246, 545

Phillips, M. M. 1993, The Astrophysical Journal Letters, 413, L105, doi: 10.1086/186970

Pimbblet, K. A. 2003, Publications of the Astronomical Society of Australia, 20, 294, doi: 10.1071/AS03043

Postman, M., & Lauer, T. R. 1995, The Astrophysical Journal, 440, 28, doi: 10.1086/175245

Pound, R. V., & Snider, J. L. 1965, Physical Review, 140, 788, doi: 10.1103/PhysRev.140.B788

Ratcliffe, H. 2010, Journal of Cosmology, 4, 693

Rauch, M. 1998, Annual Review of Astronomy and Astrophysics, 36, 267, doi: 10.1146/annurev.astro.36.1.267

Raychaudhuri, A. 1955, Physical Review, 98, 1123, doi: 10.1103/PhysRev.98.1123

Riess, A. G., Strolger, L.-G., Casertano, S., et al. 2007, The Astrophysical Journal, 659, 98, doi: 10.1086/510378

Rood, H. J. 1988, Annual Review of Astronomy and Astrophysics, 26, 245, doi: 10.1146/annurev.aa.26.090188.001333

Rood, H. J., & Struble, M. F. 1982, The Astrophysical Journal, 252, L7, doi: 10.1086/183708

Roth, K. C., & Meyer, D. M. 1995, The Astrophysical Journal, 441, 129, doi: 10.1086/175343

Sandage, A. 2010, The Astronomical Journal, 139, 728, doi: 10.1088/0004-6256/139/2/728

Sandage, A., & Lubin, L. M. 2001, The Astronomical Journal, 121, 2271, doi: 10.1086/320394

Sandage, A., & Perelmuter, J.-M. 1990, The Astrophysical Journal, 361, 1, doi: 10.1086/169161

Santangelo, N., Horstman, H., & Horstman-Moretti, E. 1973, SoPh, 29, 143, doi: 10.1007/BF00153445

Scolnic, D. M., Jones, D. O., Rest, A., et al. 2017, ArXiv e-prints. https://arxiv.org/abs/1710.00845

—. 2018, The Astrophysical Journal, 859, 101, doi: 10.3847/1538-4357/aab9bb

Sunyaev, R. A., & Zeldovich, I. B. 1980, Monthly Notices of the Royal Astronomical Society, 190, 413, doi: 10.1093/mnras/190.3.413

Sunyaev, R. A., & Zeldovich, Y. B. 1970, Astrophysics and Space Science, 9, 353, doi: 10.1007/BF00649576

Tolman, R. C. 1934, Relativity, Thermodynamics, and Cosmology

Trombka, J. I., Dyer, C. S., Evans, L. G., et al. 1977, The Astrophysical Journal, 212, 925, doi: 10.1086/155117

van Flandern, T. 1991, in Bulletin of the American Astronomical Society, Vol. 23, 1395

Watt, M. P., Ponman, T. J., Bertram, D., et al. 1992, Monthly Notices of the Royal Astronomical Society, 258, 738, doi: 10.1093/mnras/258.4.738

White, S. D. M., Briel, U. G., & Henry, J. P. 1993, Monthly Notices of the Royal Astronomical Society, 261, L8, doi: 10.1093/mnras/261.1.L8

Wolf, C., Wisotzki, L., Borch, A., et al. 2003, Astromomy and Astrophysics, 408, 499, doi: 10.1051/0004-6361:20030990

Wolf, C., Meisenheimer, K., Kleinheinrich, M., et al. 2004, Astromomy and Astrophysics, 421, 913, doi: 10.1051/0004-6361:20040525

Wood-Vasey, W. M., Friedman, A. S., Bloom, J. S., et al. 2008, The Astrophysical Journal, 689, 377, doi: 10.1086/592374

Zwicky, F. 1937, The Astrophysical Journal, 86, 217, doi: 10.1086/143864